Received: 21 July 2022 | Revised: 23 September 2022 | Accepted: 12 October 2022

DOI: 10.1002/ddr.22006

RESEARCH ARTICLE

DRUG DEVELOPMENT RESEARCH WILEY

A cytotoxic survey on *2-amino-1H-imidazol* based synthetic marine sponge alkaloid analogues

Nikolett Gémes[1,2] | Zsófia Makra[3] | Patrícia Neuperger[1] | Enikő Szabó[1] | József Á. Balog[1] | Lili Borbála Flink[4] | Beáta Kari[3] | László Hackler Jr[3] | László. G. Puskás[1,3] | Iván Kanizsai[3] | Gábor J. Szebeni[1,5]

[1]Laboratory of Functional Genomics, Biological Research Centre, Szeged, Hungary

[2]PhD School in Biology, University of Szeged, Szeged, Hungary

[3]Avidin Ltd, Szeged, Hungary

[4]Department of Dermatology and Allergology, University of Szeged, Szeged, Hungary

[5]Department of Physiology, Anatomy, and Neuroscience, Faculty of Science and Informatics, University of Szeged, Szeged, Hungary

Correspondence

Gábor J. Szebeni, Laboratory of Functional Genomics, Biological Research Centre, Temesvari krt. 62, Szeged H6726, Hungary.
Email: szebeni.gabor@brc.hu

Iván Kanizsai, Avidin Ltd., Alsó kikötő sor 11/D, Szeged H6726, Hungary.
Email: i.kanizsai@avidinbiotech.com

Funding information

2020-1.1.6-JÖVO-2021-00003; National Research, Development, and Innovation Office (NKFI), Hungary; ÚNKP-22-5 -SZTE-535 (GJS) New National Excellence Program of the Ministry for Innovation and Technology from the source of the National Research, Development and Innovation Fund; János Bolyai Research Scholarship of the Hungarian Academy of Sciences BO/00582/22/8

Abstract

Here, we describe the synthesis and biologic activity evaluation of 20 novel synthetic marine sponge alkaloid analogues with *2-amino-1H-imidazol* (2-AI) core. Cytotoxicity was tested on murine 4T1 breast cancer, A549 human lung cancer, and HL-60 human myeloid leukemia cells by the resazurin assay. A total of 18 of 20 compounds showed cytotoxic effect on the cancer cell lines with different potential. Viability of healthy human fibroblasts and peripheral blood mononuclear cells upon treatment was less hampered compared to cancer cell lines supporting tumor cell specific cytotoxicity of our compounds. The most cytotoxic compounds resulted the following IC_{50} values **28**: 2.91 µM on HL-60 cells, and **29**: 3.1 µM on 4T1 cells. The A549 cells were less sensitive to the treatments with IC_{50} 15 µM for both **28** and **29**. Flow cytometry demonstrated the apoptotic effect of the most active seven compounds inducing phosphatidylserine exposure and sub-G1 fragmentation of nuclear DNA. Cell cycle arrest was also observed. Four compounds caused depolarization of the mitochondrial membrane potential as an early event of apoptosis. Two lead compounds inhibited tumor growth in vivo in the 4T1 triple negative breast cancer and A549 human lung adenocarcinoma xenograft models. Novel marine sponge alkaloid analogues are demonstrated as potential anticancer agents for further development.

KEYWORDS

2-amino-(1H)-imidazole, 4T1 breast cancer, A549 lung cancer, HL-60 myeloid leukemia, Mannich

Iván Kanizsai and Gábor J. Szebeni have contributed equally to this work and share senior authorship.

Supporting Information Materials: Figure S1: structures were identified by ^{1}H and ^{13}C NMR spectra; Figure S2: dose-response curves of our compounds on 4T1, A549, and HL-60 cells; Figure S3: dose-response curves of our compounds on healthy human fibroblasts, and PBMCs.

1 | INTRODUCTION

Cancer is one of the leading causes of death worldwide with the reported 19.3 million new cases and death of 10 million people in 2020 (Sarfati & Gurney, 2022; Sung et al., 2021). In the European Union cancer-related deaths are expected as 1,269,200 cases in 2022 (Dalmartello et al., 2022). Cancer incidence is estimated to increase with 47% in the western countries by 2040, therefore, intensive research on the development of novel anticancer agents is highly expected (Sarfati & Gurney, 2022; Sung et al., 2021). Since 70% of the planet is covered by oceans with an estimate of 1 million unknown species, marine bioactive secondary metabolites and chemical synthesis of their derivatives may facilitate anticancer drug discovery (Anjum et al., 2016; Boucle et al., 2015). Around 30% of known bioactive compounds with marine origin are discovered from sponges with potential anticancer effects as alkaloids, sterols, terpenoids, macrolides, polyketones, peptides, glycosides, quinones (Ye et al., 2015). The wide inventory of marine sponge (phylum *Porifera*) alkaloids up to 240 already identified cytotoxic compounds as potential anticancer agents have been recently reviewed elsewhere (Elgoud Said et al., 2021; Elissawy et al., 2021). Although several marine sponge anticancer agents are reported with antiproliferative and proapoptotic effect, only few compounds, the macrolide polyketide Eribulin mesylate (Halaven) was approved for solid cancers, and nucleosides such as Fludarabin phosphate (Fludara), Nelarabin (Arranon), Cyterabine (Cytosar-U) are still approved for leukemias, lymphomas by the Food and Drug Administration (FDA) (Barreca et al., 2020; Calcabrini et al., 2017; Ercolano et al., 2019; Wang et al., 2020). Eribulin inhibits cancer cell division by targeting microtubule polymerization (Dybdal-Hargreaves et al., 2015). Fludarabine is a purine nucleoside analogue inhibiting DNA polymerases and terminating DNA replication of cancer cells (Berdis, 2017). Nelarabine also a purine nucleoside analogue as a prodrug and converted to the bioactive arabinosylguanine nucleotide triphosphate blocking DNA polymerase (Curbo & Karlsson, 2006). Cyterabine is a cytosine with arabinose sugar moiety, it blocks DNA and RNA synthesis as a pyrimidine analogue incorporating into the nucleic acid and blocking elongation. Several sponge alkaloids or chemically modified derivatives as potential anticancer agents are under development (Elgoud Said et al., 2021; Elissawy et al., 2021; Ye et al., 2015). The *2-amino-1H-imidazol* (2-AI) core is a valuable building block/fragment with natural occurrence in Sponge species. The isolated natural alkaloids show a broad range of biological activity including cytotoxic, bactericid/bacterostatic as well as antiviral effects (Figure 1) (Berlinck & Kossuga, 2005; Hoffmann & Lindel, 2003). On the account of pharmacophore character of 2-AI unit, numerous synthetic variants have been formed in the last decades highlighting the preparation of C-4/C-5 substituted 2-AI analogues (Nagasawa & Hashimoto, 2003; Weinreb, 2007). Depending on the substitution pattern, significant antimicrobial activity (against Gram-positive bacteria, *Escherichia coli* and/or *Candida albicans*) (Figure 1a), antiproliferative effects

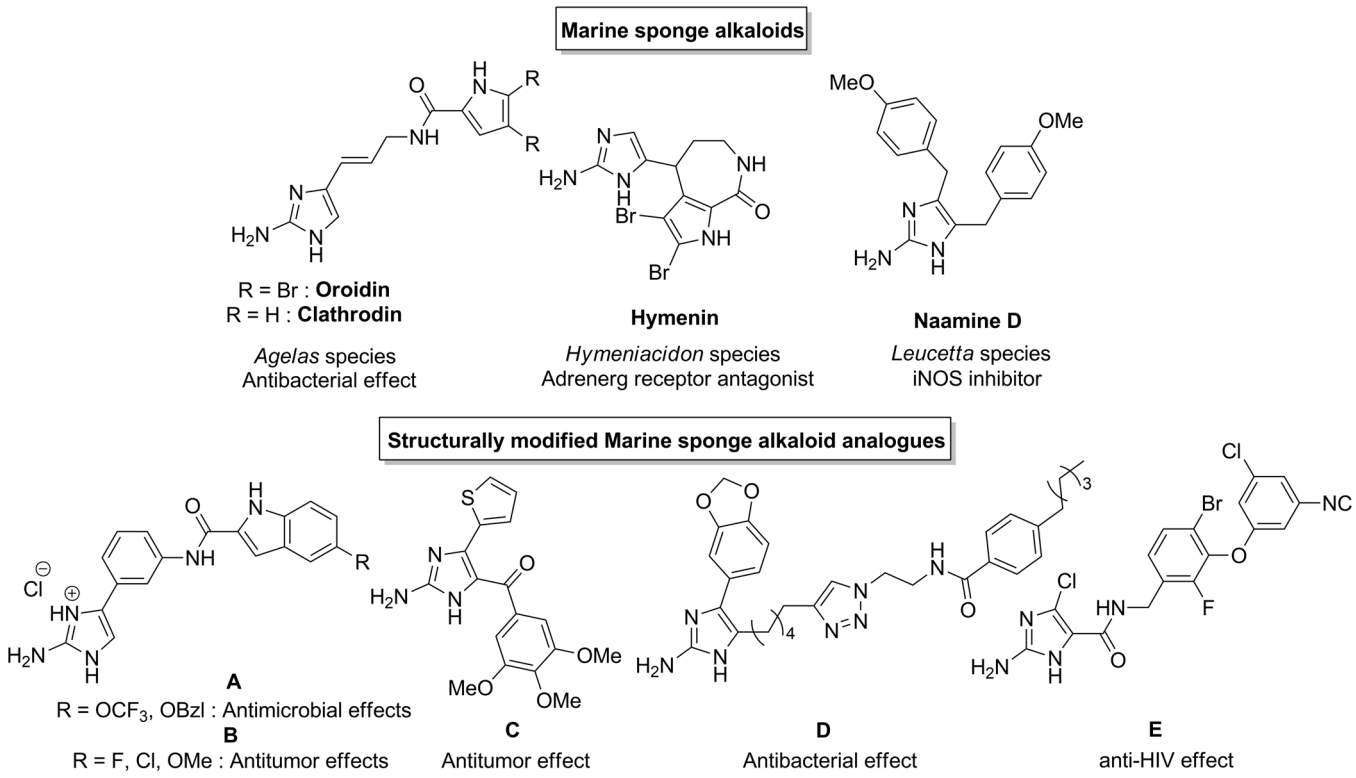

FIGURE 1 Naturally occurring marine sponge alkaloids (Oroidin, Clathrodin, Hymenin, and Naamines) and their synthetic descendants focusing on their structural modification at carbon 4 and/or 5 position

(apoptosis-inducing activities against human carcinoma cell lines) (Figure 1b), and tubulin targeting with a C-5-Aroil analogue (Figure 1c), and antibacterial activity (targeting biofilm) Figure 1d, as well as anti-HIV activity (via C-5 carboxamide function) Figure 1e) have been achieved (Chaudhary et al., 2016; Chong et al., 2012; Dyson et al., 2014; Hura et al., 2018; Su et al., 2012; Tomašič et al., 2015; Zidar et al., 2014).

Herein, we disclosed a preparation of novel synthetic marine sponge alkaloid analogues, modification on three diversity points for 2-AI score. The synthetic strategy was built on the introduction of acyl or benzoyl as well as ester substitution at C-5 position, insertion of a central linker (phenyl or Ar groups) at C-4 position and construction of a pyrrole terminal unit involving substituted indoles besides quinolines or pyridine scaffolds. Female breast cancer (11.7% of cases) and male lung cancer (11.4% of cases) are among the most frequent cancer types with high unmet medical need (Sung et al., 2021). Therefore, cytotoxic characterization and SAR (structure activity relationship) analysis of the constructed chemical library was accomplished through the investigation of 4T1 murine triple negative breast cancer cells and A549 human lung adenocarcinoma cells. Compounds were also tested on human acute myeloid (promyelocytic) leukemia HL-60 cells, because it represents one of the most frequent acute leukemia with high need for more economical, less-toxic, and more effective therapy (Wiese & Daver, 2018).

2 | MATERIALS AND METHODS

2.1 | Chemical information

2.1.1 | General information

^{1}H NMR spectra were recorded at 298 K on a Bruker Avance 500 with 5 mm BBO Prodigy Probe. Chemical shifts (δ) are given in ppm and coupling constants (*J*) are given in Hz. Chemical shifts were referenced to tetramethylsilane (δ= 0 ppm) as an internal standard. High-resolution mass spectra (HRMS) were measured on a Thermo Scientific Q Exactive hybrid quadrupole-Orbitrap mass spectrometer using HESI ion source. Samples (5 µl from 1 µg/ml solution) were injected to the MS using flow injection method (200 µl/min, acetonitrile/water = 50:50 with 0.1% TFA). TLC was performed on aluminium sheets coated with silica gel 60 F254 (1.05554; Merck). Column chromatography was performed on Kieselgel 60 (0.063–0.200 mm; Merck; elution mixture: toluene/methanol or ethyl acetate/methanol). Chemicals and solvents were commercial grade using without any purification.

2.1.2 | General procedure for the synthesis of 16–35

The corresponding carboxylic acid (1 mmol, 2 equiv.), triethylamine (139 µl, 1 mmol, 2 equiv.) and TBTU (177 mg, 0.55 mmol, 1.1 equiv.) were dissolved in dichloromethane (25 ml) and stirred at room temperature for 1 h. Then, 0.5 mmol of corresponding amine precursor was added into the reaction mixture and was stirred at ambient temperature for 72 h. Then the mixture was poured into water (50 ml) and extracted with ethyl-acetate (2 × 50 ml). The combined organic extracts were then washed with saturated $NaHCO_3$ solution (1 × 80 ml) and brine (1 × 80 ml). The organic phase was dried over Na_2SO_4, the solvent was removed at reduced pressure and the residue was subjected to the flash column chromatography (Kieselgel 60; eluents: toluene/MeOH or ethyl acetate/methanol 30:1/15:1/9:1) and recrystallization from diethyl ether/MeOH or toluene/MeOH mixture to achieve the pure target compounds.

2.1.3 | Characterization of the products 16–35

Our group published earlier the chemical synthesis of six compounds 16, 17, 19, 26, 27, 30 without the evaluation of their biologic activity, characterization of these analogues (^{1}H, ^{13}C NMR and HRMS analysis) as well as NMR spectra are found in reference (Makra et al., 2020). Structures **18, 20–25, 28–29, 31–35** were identified by 1D NMR and HRMS analysis, ^{1}H and ^{13}C NMR spectra are found in the Figure S1.

Ethyl 4-(3-(1*H*-indole-2-carboxamido)phenyl)−2-amino-1*H*-imidazole-5-carboxylate (16). The product has been showed and characterized in reference (Makra et al., 2020). NMR purity: 99+%.

Ethyl 2-amino-4-(3-(8-hydroxyquinoline-2-carboxamido)phenyl)−1*H*-imidazole-5-carboxylate (17). The product has been showed and characterized in reference (Makra et al., 2020). NMR purity: 99+%.

N-(3-(2-amino-5-benzoyl-1*H*-imidazol-4-yl)phenyl)−8-hydroxy-quinoline-2-carboxamide (18). Yellow solid, 61% yield (137 mg); Silica gel TLC Rf = 0.49 (toluene/2-propanol = 4/1); NMR purity: 99+%. ^{1}H NMR (500 MHz, dimethyl sulfoxide [DMSO]-d_6) δ = 11.06 (s, 1H), 10.45 (s, 1H), 8.58 (d, *J* = 8.6 Hz, 1H), 8.27 (d, *J* = 8.5 Hz, 1H), 8.02 (s, 1H), 7.76 (d, *J* = 8.0 Hz, 1H), 7.62 (t, *J* = 7.9 Hz, 1H), 7.54 (d, *J* = 7.9 Hz, 1H), 7.44 (d, *J* = 7.2 Hz, 2H), 7.32 (t, *J* = 7.4 Hz, 1H), 7.24 (d, *J* = 7.6 Hz, 1H), 7.18 (t, *J* = 7.6 Hz, 1H), 7.03 (t, *J* = 7.9 Hz, 1H), 6.92 (d, *J* = 7.7 Hz, 1H), 6.05 (s, 2H) ppm. ^{13}C NMR (126 MHz, DMSO-d_6) δ = 183.65, 162.39, 154.25, 153.42, 149.03, 147.77, 139.60, 138.62, 138.18, 136.88, 135.61, 131.26, 130.24, 130.20, 129.07, 128.18, 127.95, 125.82, 122.51, 121.59, 119.89, 119.44, 118.15, 112.56 ppm. HRMS (ESI) m/z: $[M + H]^+$ Calcd for $C_{26}H_{20}N_5O_3^+$ 450.1561 (100.0%), 451.1595 (28.1%); Found: 450.1554.

N-(3-(2-amino-5-benzoyl-1*H*-imidazol-4-yl)phenyl)quinoline-2-carboxamide (19). The product has been showed and characterized in reference (Makra et al., 2020). NMR purity: 97%.

N-(3-(2-amino-5-benzoyl-1*H*-imidazol-4-yl)phenyl)picolinamide (20). Yellow solid, 83% yield (159 mg); Silica gel TLC Rf = 0.41 (toluene/2-propanol = 4/1); NMR purity: 99+%. ^{1}H NMR (500 MHz, DMSO-d_6) δ = 11.02 (s, 1H), 10.36 (s, 1H), 8.75 (d, *J* = 4.2 Hz, 1H), 8.15 (d, *J* = 7.8 Hz, 1H), 8.08 (td, *J* = 7.6, 1.7 Hz, 1H), 7.96 (s, 1H), 7.69 (ddd, *J* = 7.6, 4.7, 1.3 Hz, 1H), 7.63 (d, *J* = 8.0 Hz, 1H), 7.42 (d,

J = 7.5 Hz, 2H), 7.31 (t, *J* = 7.5 Hz, 1H), 7.17 (t, *J* = 7.6 Hz, 2H), 7.02 (t, *J* = 7.8 Hz, 1H), 6.96 (d, *J* = 7.7 Hz, 1H), 6.05 (s, 2H) ppm. ^{13}C NMR (126 MHz, DMSO-d_6) δ = 183.56, 162.62, 153.40, 150.31, 149.16, 148.91, 139.62, 138.63, 138.00, 135.54, 131.20, 129.02, 128.13, 127.95, 127.38, 125.50, 122.76, 122.49, 121.32, 119.63 ppm. HRMS (ESI) m/z: $[M + H]^+$ Calcd for $C_{22}H_{18}N_5O_2^+$ 384.1455 (100.0%), 385.1489 (23.8%); Found: 384.1450.

N-(3-(2-amino-5-benzoyl-1*H*-imidazol-4-yl)phenyl)-4-bromo-1*H*-pyrrole-2-carboxamide (21). Yellow solid, 90% yield (202 mg); Silica gel TLC Rf = 0.47 (toluene/2-propanol = 4/1); NMR purity: 97%. ^{1}H NMR (500 MHz, DMSO-d_6) δ= 11.92 (s, 1H), 10.92 (s, 1H), 9.64 (s, 1H), 7.81 (s, 1H), 7.57 (d, *J* = 8.1 Hz, 1H), 7.51 – 7.43 (m, 1H), 7.39–7.32 (m, 1H), 7.21 (s, 2H), 7.17–7.12 (m, 1H), 7.10–7.06 (m, 1H), 7.04–6.86 (m, 2H), 6.74 (s, 1H), 5.92 (s, 2H) ppm. ^{13}C NMR (126 MHz, DMSO-d_6) δ = 161.39, 158.35, 139.63, 138.87, 131.27, 129.13, 128.11, 127.89, 127.21, 123.64, 122.71, 121.05, 119.41, 116.15, 113.12, 96.07, 95.66 ppm. HRMS (ESI) m/z: $[M + H]^+$ Calcd for $C_{21}H_{17}BrN_5O_2^+$ 450.0561 (100.0%), 452.0540 (97.3%), 451.0594 (22.7%), 453.0574 (22.1%), 452.0628 (2.5%), 454.0607 (2.4%), 451.0531 (1.8%), 453.0511 (1.8%); Found: 450.0553, 452.0532, 451.0586, 453.0563.

N-(3-(2-amino-5-benzoyl-1*H*-imidazol-4-yl)phenyl)-1*H*-pyrrole-2-carboxamide (22). Yellow solid, 54% yield (100 mg); Silica gel TLC Rf = 0.41 (toluene/2-propanol = 4/1); NMR purity: 97%. ^{1}H NMR (500 MHz, DMSO-d_6) δ= 11.58 (s, 1H), 10.98 (s, 1H), 9.58 (s, 1H), 7.82 (s, 1H), 7.59 (d, *J* = 8.1 Hz, 1H), 7.48–6.80 (m, 9H), 6.16 (d, *J* = 3.4 Hz, 1H), 5.99 (s, 2H) ppm. ^{13}C NMR (126 MHz, DMSO-d_6) δ = 159.44, 139.60, 139.23, 131.28, 129.37, 128.68, 128.12, 126.57, 122.91, 120.95, 119.30, 111.73, 109.34 ppm. HRMS (ESI) m/z: $[M + H]^+$ Calcd for $C_{21}H_{18}N_5O_2^+$ 372.1455 (100.0%), 373.1489 (22.7%); Found: 372.1448.

N-(3-(2-amino-5-benzoyl-1*H*-imidazol-4-yl)phenyl)-5-fluoro-1*H*-indole-2-carboxamide (23). Yellow solid, 50% yield (110 mg); Silica gel TLC Rf = 0.43 (toluene/2-propanol = 4/1); NMR purity: 90%. ^{1}H NMR (500 MHz, DMSO-d_6) δ= 11.80 (s, 1H), 11.02 (s, 1H), 10.09 (s, 1H), 7.86 (t, *J* = 1.9 Hz, 1H), 7.62 (d, *J* = 7.1 Hz, 1H), 7.49–7.38 (m, 6H), 7.33 (t, *J* = 7.4 Hz, 1H), 7.18 (t, *J* = 7.7 Hz, 2H), 7.09 (td, *J* = 9.3, 2.5 Hz, 1H), 7.00 (t, *J* = 7.9 Hz, 1H), 6.90 (d, *J* = 7.7 Hz, 1H), 6.03 (s, 2H) ppm. ^{13}C NMR (126 MHz, DMSO-d_6) δ = 183.61, 159.65, 157.68 (d, *J* = 231.9 Hz), 153.38, 149.14, 139.57, 138.68, 135.50, 133.98, 133.68, 131.24, 129.06, 128.15, 127.89, 127.57 (d, *J* = 10.3 Hz), 125.24, 122.44, 121.28, 119.51, 114.06 (d, *J* = 10.0 Hz), 112.95 (d, *J* = 27.0 Hz), 106.35 (d, *J* = 22.8 Hz), 104.22 (d, *J* = 3.4 Hz) ppm. HRMS (ESI) m/z: $[M + H]^+$ Calcd for $C_{25}H_{19}FN_5O_2^+$ 440.1518 (100.0%), 441.1551 (27.0%); Found: 440.1509.

Ethyl 2-amino-4-(3-(5-methoxy-1*H*-indole-2-carboxamido)phenyl)-1*H*-imidazole-5-carboxylate (24). Pale yellow solid, 58% yield (122 mg); Silica gel TLC Rf = 0.39 (toluene/2-propanol = 4/1); NMR purity: 99%. ^{1}H NMR (500 MHz, DMSO-d_6) δ= 11.56 (s, 1H), 10.85 (s, 1H), 10.18 (s, 1H), 8.26 (s, 1H), 7.77 (d, *J* = 8.0 Hz, 1H), 7.70 (d, *J* = 7.8 Hz, 1H), 7.37 (d, *J* = 4.0 Hz, 1H), 7.36 (d, *J* = 2.5 Hz, 1H), 7.34 (t, *J* = 8.0 Hz, 1H), 7.14 (d, *J* = 2.4 Hz, 1H), 6.89 (dd, *J* = 9.0, 2.5 Hz, 1H), 5.77 (s, 2H), 4.19 (q, *J* = 7.1 Hz, 2H), 3.79 (s, 3H), 1.24 (t, *J* = 7.1 Hz, 3H). ^{13}C NMR (126 MHz, DMSO-d_6) δ = 160.07, 159.91, 154.32, 152.09, 146.35, 138.71, 135.15, 132.57, 132.32, 128.07, 127.86, 124.79, 121.41, 120.20, 115.47, 113.67, 112.04, 104.01, 102.58, 59.82, 55.77, 14.74 ppm. HRMS (ESI) m/z: $[M + H]^+$ Calcd for $C_{22}H_{22}N_5O_4^+$ 420.1667 (100.0%), 421.1700 (23.8%); Found: 420.1663.

N-(3-(2-amino-5-benzoyl-1*H*-imidazol-4-yl)phenyl)-1*H*-indole-2-carboxamide (25). Yellow solid, 52% yield (109 mg); Silica gel TLC Rf = 0.45 (toluene/2-propanol = 4/1); NMR purity: 91%. ^{1}H NMR (500 MHz, DMSO-d_6) δ= 11.69 (s, 1H), 11.02 (s, 1H), 10.05 (s, 1H), 7.88 (s, 1H), 7.68 (d, *J* = 8.0 Hz, 1H), 7.63 (d, *J* = 9.0 Hz, 1H), 7.48 (d, *J* = 8.3 Hz, 1H), 7.43 (d, *J* = 7.1 Hz, 2H), 7.42–7.40 (m, 1H), 7.33 (t, *J* = 7.4 Hz, 1H), 7.23 (t, *J* = 7.6 Hz, 1H), 7.19 (t, *J* = 7.7 Hz, 2H), 7.08 (t, *J* = 7.5 Hz, 1H), 6.99 (t, *J* = 7.9 Hz, 1H), 6.89 (d, *J* = 7.7 Hz, 1H), 6.04 (s, 2H) ppm. ^{13}C NMR (126 MHz, DMSO-d_6) δ = 183.61, 159.96, 153.39, 149.19, 139.57, 138.80, 137.25, 135.49, 131.98, 131.25, 129.07, 128.15, 127.88, 127.52, 125.15, 124.21, 122.44, 122.23, 121.22, 120.36, 119.46, 112.85, 104.24 ppm. HRMS (ESI) m/z: $[M + H]^+$ Calcd for $C_{25}H_{20}N_5O_2^+$ 422.1612 (100.0%), 423.1646 (27.0%); Found: 422.1607.

N-(3-(5-acetyl-2-amino-1*H*-imidazol-4-yl)phenyl)-5-methoxy-1*H*-indole-2-carboxamide (26). The product has been showed and characterized in reference (Makra et al., 2020). NMR purity: 99+%.

N-(3-(2-amino-5-benzoyl-1*H*-imidazol-4-yl)phenyl)-5-methoxy-1*H*-indole-2-carboxamide (27). The product has been showed and characterized in reference (Makra et al., 2020). NMR purity: 99+%.

N-(3-(2-amino-5-benzoyl-1*H*-imidazol-4-yl)phenyl)-5-bromo-1*H*-indole-2-carboxamide (28). Yellow solid, 70% yield (175 mg); Silica gel TLC Rf = 0.47 (toluene/2-propanol = 4/1); NMR purity: 95+%. ^{1}H NMR (500 MHz, DMSO-d_6) δ= 11.91 (s, 1H), 11.03 (s, 1H), 10.14 (s, 1H), 7.93 (s, 1H), 7.86 (s, 1H), 7.62 (d, *J* = 7.1 Hz, 1H), 7.47–7.38 (m, 4H), 7.34 (dd, *J* = 8.7, 1.9 Hz, 2H), 7.19 (t, *J* = 6.4 Hz, 2H), 7.00 (t, *J* = 7.1 Hz, 1H), 6.91 (d, *J* = 7.6 Hz, 0H), 6.04 (s, 2H) ppm. ^{13}C NMR (126 MHz, DMSO-d_6) δ = 183.61, 159.57, 153.38, 149.13, 139.56, 138.65, 135.83, 135.49, 133.27, 131.26, 129.30, 129.07, 128.14, 127.92, 126.79, 125.27, 124.38, 122.45, 121.27, 119.52, 114.87, 112.80, 103.66 ppm. HRMS (ESI) m/z: $[M + H]^+$ Calcd for $C_{25}H_{19}BrN_5O_2^+$ 500.0717 (100.0%), 502.0697 (97.3%), 501.0751 (27.0%), 503.0730 (26.3%), 502.0784 (3.5%), 504.0764 (3.4%), 501.0687 (1.8%), 503.0667 (1.8%); Found: 500.0707, 501.0737, 502.0686, 503.0716, 504.0744.

N-(3-(2-amino-5-benzoyl-1*H*-imidazol-4-yl)phenyl)-5-chloro-1*H*-indole-2-carboxamide (29). Yellow solid, 58% yield (132 mg); Silica gel TLC Rf = 0.45 (toluene/2-propanol = 4/1); NMR purity: 98%. ^{1}H NMR (500 MHz, DMSO-d_6) δ= 11.84 (s, 1H), 10.94 (s, 1H), 10.08 (s, 1H), 7.87 (s, 1H), 7.77 (s, 1H), 7.63 (d, *J*= 7.8 Hz, 1H), 7.53–7.29 (m, 5H), 7.28–7.14 (m, 3H), 7.01 (t, *J* = 7.8 Hz, 1H), 6.94 (d, *J* = 7.9 Hz, 1H), 5.97 (s, 2H) ppm. ^{13}C NMR (126 MHz, DMSO-d_6) δ = 183.61, 159.60, 153.33, 149.07, 139.63, 138.66, 135.67, 135.53, 133.53, 131.20, 129.03, 128.59, 128.12, 127.89, 125.26, 124.89, 124.29, 122.47, 121.37, 121.24, 119.60, 114.45, 103.82 ppm. HRMS (ESI) m/z: $[M + H]^+$ Calcd for $C_{25}H_{19}ClN_5O_2^+$ 456.1222 (100.0%), 458.1193

(32.0%), 457.1256 (27.0%), 459.1226 (8.6%); Found: 456.1214, 457.1245, 458.1175, 459.1212.

N-(3-(5-acetyl-2-amino-1*H*-imidazol-4-yl)phenyl)-5-fluoro-1*H*-indole-2-carboxamide (30). The product has been showed and characterized in reference (Makra et al., 2020). NMR purity: 99+%.

Ethyl 2-amino-4-(3-(5-fluoro-1*H*-indole-2-carboxamido)phenyl)-1*H*-imidazole-5-carboxylate (31). Pale yellow solid, 40% yield (81 mg); Silica gel TLC Rf = 0.35 (toluene/2-propanol = 4/1); NMR purity: 91%. ^{1}H NMR (500 MHz, DMSO-d_6) δ= 11.82 (s, 1H), 10.85 (s, 1H), 10.28 (s, 1H), 8.26 (s, 1H), 7.77 (d, *J* = 9.2 Hz, 1H), 7.71 (d, *J* = 7.9 Hz, 1H), 7.51–7.46 (m, 1H), 7.46 (d, *J* = 3.5 Hz, 1H), 7.45 (d, *J* = 1.8 Hz, 1H), 7.34 (t, *J* = 7.9 Hz, 1H), 7.09 (td, *J* = 9.3, 2.5 Hz, 1H), 5.77 (s, 2H), 4.19 (q, *J* = 7.1 Hz, 2H), 1.24 (t, *J* = 7.1 Hz, 3H) ppm. ^{13}C NMR (126 MHz, DMSO-d_6) δ = 159.90, 159.81, 157.68 (d, *J* = 233.3 Hz), 152.09, 146.31, 138.57, 135.18, 133.98, 133.74, 128.11, 127.60 (d, *J* = 10.4 Hz), 124.94, 121.44, 120.23, 114.05 (d, *J* = 9.9 Hz), 112.93 (d, *J* = 26.5 Hz), 112.05, 106.34 (d, *J* = 22.7 Hz), 104.26 (d, *J* = 5.4 Hz) ppm. HRMS (ESI) m/z: $[M + H]^+$ Calcd for $C_{21}H_{19}FN_5O_3^+$ 408.1467 (100.0%), 409.1500 (22.7%); Found: 408.1461.

N-(3-(2-amino-5-benzoyl-1*H*-imidazol-4-yl)-4-chlorophenyl)-5-bromo-1*H*-indole-2-carboxamide (32). Yellow solid, 33% yield (88 mg); Silica gel TLC Rf = 0.52 (toluene/2-propanol = 4/1); NMR purity: 99+%. ^{1}H NMR (500 MHz, DMSO-d_6) δ= 11.88 (s, 1H), 11.14 (s, 1H), 10.18 (s, 1H), 7.93 (s, 1H), 7.70 (s, 1H), 7.63 (d, *J* = 8.4 Hz, 1H), 7.45 (d, *J*= 8.7 Hz, 1H), 7.39 (s, 1H), 7.37–7.33 (m, 3H), 7.24 (t, *J* = 7.0 Hz, 1H), 7.14 (d, *J* = 8.7 Hz, 1H), 7.09 (t, *J* = 7.3 Hz, 2H), 6.01 (s, 2H) ppm. ^{13}C NMR (126 MHz, DMSO-d_6) δ = 183.41, 159.67, 153.52, 146.40, 139.05, 137.65, 135.96, 135.19, 133.01, 130.98, 129.38, 129.27, 128.58, 127.57, 127.28, 126.94, 124.41, 123.91, 123.85, 120.95, 114.90, 112.88, 103.93 ppm. HRMS (ESI) m/z: $[M + H]^+$ Calcd for $C_{25}H_{18}BrClN_5O_2^+$ 534.0327 (100.0%), 536.0307 (97.3%), 536.0298 (32.0%), 538.0277 (31.1%), 535.0361 (27.0%), 537.0340 (26.3%), 537.0331 (8.6%), 539.0311 (8.4%), 536.0394 (3.5%), 538.0374 (3.4%), 535.0298 (1.8%), 537.0277 (1.8%), 538.0365 (1.1%), 540.0345 (1.1%); Found: 534.0316, 535.0346, 536.0294, 537.0323, 538.255, 539.0294.

N-(3-(2-amino-5-benzoyl-1*H*-imidazol-4-yl)-5-chlorophenyl)-5-bromo-1*H*-indole-2-carboxamide (33). Yellow solid, 28% yield (75 mg); Silica gel TLC Rf = 0.56 (toluene/2-propanol = 4/1); NMR purity: 99+%. ^{1}H NMR (500 MHz, DMSO-d_6) δ= 11.88 (s, 1H), 11.04 (s, 1H), 10.25 (s, 1H), 7.94 (d, *J* = 1.5 Hz, 1H), 7.84 (s, 1H), 7.79 (s, 1H), 7.48 (s, 1H), 7.45 (d, *J* = 8.9 Hz, 2H), 7.42–7.36 (m, 2H), 7.36 (dd, *J* = 8.7, 1.9 Hz, 1H), 7.26 (t, *J* = 7.5 Hz, 2H), 6.99 (s, 1H), 6.01 (s, 2H) ppm. ^{13}C NMR (126 MHz, DMSO-d_6) δ = 183.65, 159.80, 153.35, 147.26, 139.98, 139.56, 137.12, 136.00, 132.87, 132.38, 131.50, 129.26, 128.94, 128.31, 127.02, 124.47, 122.77, 119.51, 118.79, 114.92, 112.90, 104.10 ppm. HRMS (ESI) m/z: $[M + H]^+$ Calcd for $C_{25}H_{18}BrClN_5O_2^+$ 534.0327 (100.0%), 536.0307 (97.3%), 536.0298 (32.0%), 538.0277 (31.1%), 535.0361 (27.0%), 537.0340 (26.3%), 537.0331 (8.6%), 539.0311 (8.4%), 536.0394 (3.5%), 538.0374 (3.4%), 535.0298 (1.8%), 537.0277 (1.8%), 538.0365 (1.1%), 540.0345 (1.1%); Found: 534.0320, 536.0298, 535.0348, 537.0323, 538.0257, 539.0292.

N-(3-(2-amino-5-benzoyl-1*H*-imidazol-4-yl)-4-methylphenyl)-5-bromo-1*H*-indole-2-carboxamide (34). Pale yellow solid, 82% yield (211 mg); Silica gel TLC Rf = 0.45 (toluene/2-propanol = 4/1); NMR purity: 95+%. ^{1}H NMR (500 MHz, DMSO-d_6) δ= 11.83 (s, 1H), 10.99 (s, 1H), 9.92 (s, 1H), 7.93–7.88 (m, 1H), 7.50 (d, *J* = 7.6 Hz, 1H), 7.44 (d, *J* = 8.8 Hz, 1H), 7.42 (s, 1H), 7.37–7.30 (m, 2H), 7.30 (d, *J* = 7.0 Hz, 2H), 7.20 (t, *J* = 6.8 Hz, 1H), 7.04 (t, *J* = 6.8 Hz, 2H), 6.95 (d, *J* = 7.9 Hz, 1H), 5.99 (s, 2H), 2.09 (s, 3H) ppm. ^{13}C NMR (126 MHz, DMSO-d_6) δ = 183.29, 159.36, 153.51, 149.75, 139.16, 136.28, 135.83, 135.63, 133.43, 131.70, 130.77, 129.89, 129.33, 128.49, 127.52, 126.69, 124.29, 123.77, 122.88, 119.54, 114.85, 112.78, 103.49, 19.57 ppm. HRMS (ESI) m/z: $[M + H]^+$ Calcd for $C_{26}H_{21}BrN_5O_2^+$ 514.0874 (100.0%), 516.0853 (97.3%), 515.0907 (28.1%), 517.0887 (27.4%), 516.0941 (3.8%), 518.0920 (3.7%), 515.0844 (1.8%), 517.0824 (1.8%); Found: 514.0862, 516.0839, 515.0893, 517.0873, 518.0904.

N-(4-(2-amino-5-benzoyl-1*H*-imidazol-4-yl)phenyl)-5-bromo-1*H*-indole-2-carboxamide (35). Yellow solid, 30% yield (75 mg); Silica gel TLC Rf = 0.35 (toluene/2-propanol = 4/1); NMR purity: 93%. ^{1}H NMR (500 MHz, DMSO-d_6) δ= 11.91 (s, 1H), 10.25 (s, 1H), 7.91 (s, 1H), 7.62 (d, *J* = 8.6 Hz, 2H), 7.55 (d, *J* = 7.3 Hz, 2H), 7.47–7.32 (m, 6H), 7.28 (t, *J* = 7.6 Hz, 2H), 6.13 (s, 2H) ppm. ^{13}C NMR (126 MHz, DMSO-d_6) δ = 184.24, 159.70, 152.23, 139.49, 138.92, 135.93, 133.23, 131.56, 129.96, 129.29, 129.27, 128.31, 126.86, 124.36, 119.41, 114.88, 112.84, 103.93 ppm. HRMS (ESI) m/z: $[M + H]^+$ Calcd for $C_{25}H_{19}BrN_5O_2^+$ 500.0717 (100.0%), 502.0697 (97.3%), 501.0751 (27.0%), 503.0730 (26.3%), 502.0784 (3.5%), 504.0764 (3.4%), 501.0687 (1.8%), 503.0667 (1.8%); 500.0702, 501.0736, 502.0679, 503.0714.

2.2 | Cell culturing

The A549 human non-small cell lung cancer cell line, the human HL-60 promyelocytic leukemia cell line, and the 4T1 murine triple negative breast cancer cell line was purchased from the American Type Culture Collection. Cells were maintained in the following media: A549 cells in Dulbecco's modified Eagle medium (DMEM)/F12 (containing 3.151 g/L glucose), RPMI (containing 2 g/L glucose) for the HL-60 or 4T1 cell lines. Media were purchased from Capricorn Scientific GmbH and supplemented with 10% fetal bovine serum (Euroclone, Peri), 2 mM GlutaMAX (Gibco), 100 U/ml penicillin, and 100 µg/ml streptomycin antibiotics (penicillin G sodium salt and streptomycin sulfate salt; Merck). The cells were cultured in a standard tissue culture Petri dish, 10 mm in diameter (Corning Life Sciences) at maximum 80% confluence in a standard atmosphere of 95% air and 5% CO_2 (Sanyo).

2.3 | Isolation of primary human fibroblasts

Human primary skin fibroblasts were isolated as described previously (Szebeni et al., 2018). Briefly, healthy volunteers (age 18–60 years) were enrolled into the study. The punch biopsies were taken from

healthy subjects from the breast area undergoing plastic surgery. Primary fibroblasts were obtained from the skin by enzymatic digestion according to a standard protocol. Briefly, skin specimens were first washed in Salsol A solution (Human Rt) supplemented with 2% antibiotic/antimycotic solution (Sigma-Aldrich). Skin samples were then cut into narrow strips and incubated in Dispase solution (Roche Diagnostics, Mannheim, Germany) overnight at 4°C. The epidermis was subsequently separated from the dermis. Fibroblasts were obtained by incubating the dermis in Digestion Mix solution (Sigma-Aldrich, Collagenase, Hyaluronidase, and Deoxyribonuclease) at 37°C for 2 h. Cell suspensions were filtered through a 100 µm nylon mesh (BD Falcon), and cells were pelleted by centrifugation (Megafuge 16; Thermo Fisher Scientific). Fibroblasts were grown in low glucose DMEM/F12 medium containing 15% FCS, 1% antibiotic/antimycotic (PAA, Pasching, Austria) and 1% L-glutamine solution (PAA). Fibroblasts were cultured at 37°C and 5% CO_2 in humidified conditions. Depending on the cell growth, the medium was changed every 2–4 days, and cells were passaged at 80% of confluence.

2.4 | Isolation of peripheral blood mononuclear cells (PBMCs)

The PBMCs were isolated from the peripheral blood of healthy volunteers as described previously (Szebeni et al., 2022). Briefly, the withdrawal of 20 ml peripheral blood was carried out into ethylenediaminetetraacetic acid (EDTA) Vacutainers (Beckton Dickinson). PBMCs were isolated by Ficoll density gradient centrifugation using Leucosep tubes (Greiner Bio-One). Cells were pelleted by centrifugation at 800*g* for 20 min. The ring of PBMCs was harvested by pipetting and diluted with 15 ml phosphate buffered saline (PBS), then centrifuged at 350*g* for 5 min. The supernatant (S/N) was removed. If necessary, red blood cells were lysed by 2 ml ACK solution (prepared in our laboratory: 0.15 M NaH_4Cl, 10 mM $KHCO_3$, 0.1 mM Na_2EDTA, pH7.4; Merck) at room temperature (RT) for 2 min. Cells were washed with 15 ml PBS and centrifuged at 350*g* for 5 min. Cells were resuspended in complete RPMI-1640 cell culture media (Lonza) containing 10% FCS (Euroclone), 100 U/ml penicillin sodium salt and 100 µg/ml streptomycin sulfate salt (Merck). The cells were plated for the treatment as described in the relevant Sections of Materials and Methods (Section 2).

2.5 | Human ethical clearance

The subjects gave their informed consent for inclusion before participating in the study. The study was conducted in accordance with the Declaration of Helsinki, and the protocol was approved for the isolation of human fibroblast by the Regional and Institutional Research Ethics Committee (2799, 3517). The protocol was approved for the isolation of human PBMCs by the National Institute of Environmental Health under the 47226-7/2019/EÜIG (2019) ethical license. Informed consent was obtained from all subjects involved in the study.

2.6 | Resazurin cell viability assay

Viability of the cells was measured using the resazurin assay as described previously (Demjen et al., 2018; Szebeni et al., 2017, 2018). Briefly, the healthy human primary fibroblasts (6000), A549 (10,000), HL-60 (20,000), 4T1 (10,000), PBMCs (200,000) were seeded into 96-well plates (Corning Life Sciences) in media. Adherent cells were cultured overnight before treatment. Compounds were dissolved in DMSO at 10 mM concentration. Serial dilutions were made in cell culture media freshly. Effects of the compounds were examined in the following concentrations: 1.56, 3.13, 6.25, 12.5, 25, and 50 µM in 100 µl after 72 h incubation. The most active compounds 23, 27, 28, 29, 32, 33, and 35 were tested in the following concentrations: 390 nM, 780 nM, 1.56 µM, 3.13 µM, 6.25 µM, 12.5 µM for the treatment of HL-60 cells for 72 h. Resazurin reagent (Merck) was dissolved in PBS (pH 7.4) at 0.15 mg/ml concentration, sterile filtered (0.22 µm, Merck Millipore), and aliquoted at −20°C. We applied resazurin 20 µl stock to 100 µl/well culture. After 2 h incubation at 37°C, 5% CO_2 (Sanyo) fluorescence (530 nm excitation/580 nm emission) was recorded on a multimode microplate reader (Biotek Synergy H1; Agilent). Viability was calculated with relation to untreated control cells (1 corresponds to 100% viability on the y axis), and blank wells containing media without cells. IC_{50} values (50% inhibiting concentration) were calculated by GraphPad Prism® (version 8).

2.7 | Flow cytometry

2.7.1 | Detection of phosphatidylserine exposure

Apoptosis was detected as described previously (Demjen et al., 2018). Briefly, HL-60 cells (100,000) were treated with the compounds for 24 h. Briefly, cells cultured under different conditions were collected and resuspended in Annexin V binding buffer (0.01 M HEPES, 0.14 M NaCl and 2.5 mM $CaCl_2$, Merck). Annexin V-Alexa 488 (2.5:100; Thermo Fisher Scientific) was added to the cells, which were then kept in the dark at room temperature for 15 min. Before the acquisition, propidium iodide (10 µg/ml) (Sigma-Aldrich) was added in Annexin V binding buffer to dilute Annexin V-Alexa 488 5X. Cells were acquired on a Cytoflex S cytofluorimeter (Beckman Coulter) and analysed using CytExpert software (version 2.4; Beckman Coulter). The percentage of the AnnexinV-Alexa 488, (AnnV) negative and propidium iodide, (PI) negative living cells (AnnV−/PI−), the early apoptotic (AnnV+/PI−), late apoptotic (AnnV+/PI+) and necrotic (AnnV−/PI+) cells were determined. Data were visualized by GraphPad Prism®.

2.7.2 | Sub-G1 and cell cycle analysis

Cell cycle analysis was performed as described previously (Alfoldi et al., 2019). Briefly, the HL-60 cells (100,000) treated with compounds were collected after 72 h, washed with PBS and resuspended in DNA binding buffer (1X PBS, 0.1% tri-sodium-citrate, 10 µg/ml PI, 0.1% Triton X-100, 10 µg/ml RNaseA; Merck). After 30 min incubation at room temperature cells were acquired on a Cytoflex S cytofluorimeter, sub-G1 apoptotic population and cell cycle phases were analyzed using CytExpert software. Doublets were gated out for cell cycle analysis which was based on FSC-H/FSC-W dot plots. Data were visualized by GraphPad Prism®.

2.7.3 | Detection of the mitochondrial membrane depolarization

The change of the mitochondrial membrane polarization was detected as described previously (Kanizsai et al., 2018; Kotogany et al., 2020). Briefly, HL-60 cells (1×10^5) were plated in 24-well tissue culture plates (Corning Life Sciences) in RPMI 10% FCS and were treated in 500 µl media containing test compounds. Untreated control cells were supplemented with 500 µl cell culture media. After 16 h, the supernatants were harvested. Cells were washed with PBS, trypsinized, pooled with the corresponding supernatant, and centrifuged (2000 rpm, 5 min). The pellet was resuspended and incubated in 5 µg/ml JC-1 (5,5′,6,6′-tetrachloro-1,1′,3,3′-tetraethylbenzimidazolocarbocyanine iodide for 15 min, Chemodex) containing media in final volume 300 µl at 37°C. Finally, using PE (585/42 nm) - FITC (525/40 nm) channels, the red-green fluorescence intensity of 2×10^4 events was acquired immediately on a Cytoflex S flow cytometer. Data were analyzed using CytExpert software gating out debris. Bar graphs show the percentage of green positive cells visualized by GraphPad Prism® 8.

2.8 | In vivo tumor models

2.8.1 | The A549 xenograft assay

The A549 xenograft assay was performed as described previously (Puskás et al., 2016). Briefly, tumor cells were cultured, counted, and resuspended in sterile PBS at a concentration of 4.5×10^7 cells/ml. A volume of 100 µl (4.5×10^6 cells, respectively) was injected subcutaneously into the flanks of NOD SCID (NOD.Cg-Prkdc^{scid}Il2rg^{tm1Wjl}/SzJ, Innovo Ltd.) mice at an age of 6 weeks. Mice were kept in individual ventilated cages to avoid infection. All mice were fed a commercial sterile diet and water ad libitum and were housed in an animal facility under a 12-h light/dark cycle at constant temperature and humidity. The study was performed according to the Institutional and National Animal Experimentation and Ethics Guidelines under ethical clearance (XXIX./3610/2012). Common vehicle of compound 28 consisting of 80% Peg-200 (Merck) and 20% Chremophor EL (BASF) was dissolved in water for injection in 1:8 final ratio. After growth of tumors to an average of 20 mm^3 and randomization into groups, 10 mice per treatment group were treated with 60 mg/kg of 28 daily in 100 µl intraperitoneally; or one dose of 5 mg/kg cisplatin (Platidiam, 0.5 mg/ml, TEVA Hungary) intraperitoneally in every fourth day. The health of these mice was monitored every day and tumor sizes were measured periodically (in every 2 days) using digital calipers until sacrifice. Tumor volumes were calculated by the formula $0.5 \times d^2 \times D$, where d = minor diameter, D= major diameter. Animal weights were measured throughout the study to monitor toxicity. Arithmetic means and standard error of the mean (SEM) values were determined in MS Excel (Microsoft Corp.).

2.8.2 | The 4T1 murine breast cancer model

The 4T1 triple negative murine breast cancer model was performed as described previously (Balog et al., 2019). Briefly, the animal experiments were performed in accordance with animal experimentation and ethics guidelines of the EU (2010/63/EU). Experimental protocols were approved by the responsible governmental agency (National Food Chain Safety Office) in possession of an ethical clearance XXIX./128/2013. Female Charles River-derivative BALB/c mice (8–10 weeks old) were purchased from Kobay Ltd., (Ankara, Turkey) and were injected orthotopically with 4T1 breast carcinoma cells (1×10^5 cells in 100 µl FCS free RPMI). The animals had free access to food and water. Ten mice were included into each experimental group. Common vehicle of compounds consisting of 80% Peg-200 (Merck) and 20% Chremophor EL (BASF) was dissolved in water for injection in 1:8 final ratio. After growth of tumors to an average of 20 mm^3 and randomization into groups, 10 mice per treatment group were treated with 60 mg/kg of 28 or 29 daily in 100 µl intraperitoneally. Treatment by cisplatin (Platidiam, 0.5 mg/ml, TEVA Hungary) was started after 10 days of inoculation and followed in every 4th day in 4 mg/kg dose administered intraperitoneally once on the day of the treatment. Tumors were evaluated macroscopically by the following parameters: (1) incidence of palpable tumors was determined by the daily monitoring of animals in each experimental group; (2) tumor size was measured with a precision caliper and calculated according to the formula: $0.5 \times d^2 \times D$; where d = minor diameter, D= major diameter. Mice showing signs of suffering (lost 15% of body weight and/or loss of the righting reflex and/or enable to eat, drink) due to (ethical) legislation were sacrificed. Animal weights were measured throughout the study to monitor toxicity. Arithmetic means and SEM values were determined in MS Excel.

2.9 | Statistical analysis

Significance of differences between groups was determined by two-tailed Student's *t* test in Microsoft Excel in a paired comparison with the untreated samples in the assays of cells. For the in vivo

experiments, the distribution of data was examined by the D'Agostino & Pearson test in GraphPad Prism. The data of 4T1 model showed normal distribution with 4× deviation differences among the groups, therefore multiple comparison was performed by the Brown-Forsythe and Welch analysis of variance (ANOVA) by controlling the False Discovery Rate, test: Two stage Benjamini-Krieger-Yekutieli, Q [Desired false discovery rate] = 0.1. The data of A549 model showed normal distribution with similar deviation among the groups, therefore multiple comparison was performed by the Ordinary one-way ANOVA by controlling the false discovery rate as above.

3 | RESULTS

3.1 | Chemical synthesis of the 2-amino-1H-imidazole compounds and structure activity relationship

To obtain potentially cytotoxic compounds, a simple and convenient multistep synthetic pathway has been developed starting from 2-amino pyrimidine scaffold towards structurally modified sponge alkaloid analogues **16–35**. Following multistep procedure involving Mannich-3CR, intramolecular oxidative annulation, a reduction step and finally an amine coupling sequence, a diversely structured chemical library has been constructed, with varying substituents in three positions (Figure 2).

In each step, the applied methods have been accomplished by slight modification of the selected literature procedures. The **1a-g** Mannich products have been prepared in yields of 30%–90%, next, the corresponding nitro intermediates **2–8** were isolated in poor to high yields (20%–95%). The reduction step of **2–8** was carried out by $SnCl_2$ induction in concentrated HCl to form the **9–15** 3-aminophenyl intermediates (yields: 62%–92%). Finally, primary amine coupling mediated by TEA/TBTU gave the target amides **16–35** in yields up to 90%.

The cytotoxic characterization of the 20-membered alkaloid library has revealed a moderate to weak antitumor activity against 4T1, A549 and HL-60 cancer cell lines. As biological assessment shows, the insertion of indole moiety at the R^3 position exposed a potential hit compound. Although a moderate HL-60 effect was demonstrated with the inclusion of 8-hydroxiquinoline in combination with R^1= OEt (17, IC_{50} = 5.81 μM), remarkable cytotoxicity was detected only for **23**. In case of **23**, the introduction of C-7-fluorine substituted indole and R^1 = Ph contribute for the higher cytotoxic potential against the evaluated cancer cell lines such as 4T1 (IC_{50} = 9.05 μM) as well as HL-60 (IC_{50} = 5.21 μM). Unfortunately, other indole analogues 16 and 24 with R^1 = OEt showed a significantly decreased antitumor level with 12.61–34.63 μM IC_{50} values, with **24** showing a moderate potential on HL-60 cell line (IC_{50} = 7.57 μM). In addition, other five or six-membered rings like pyrroles and pyridines as well as quinoline moieties at R^3 exhibited diminished cytotoxic effects (Figure 3).

As a continuation, further seven analogues **25–31** have been prepared by incorporating either R^1= Ac or Bz as well as R^3 = indole units decorated with EWG (halogenides) or ED (OMe) groups at C-7 (Figure 4). Insertion of chlorine (for **29**) instead of fluorine

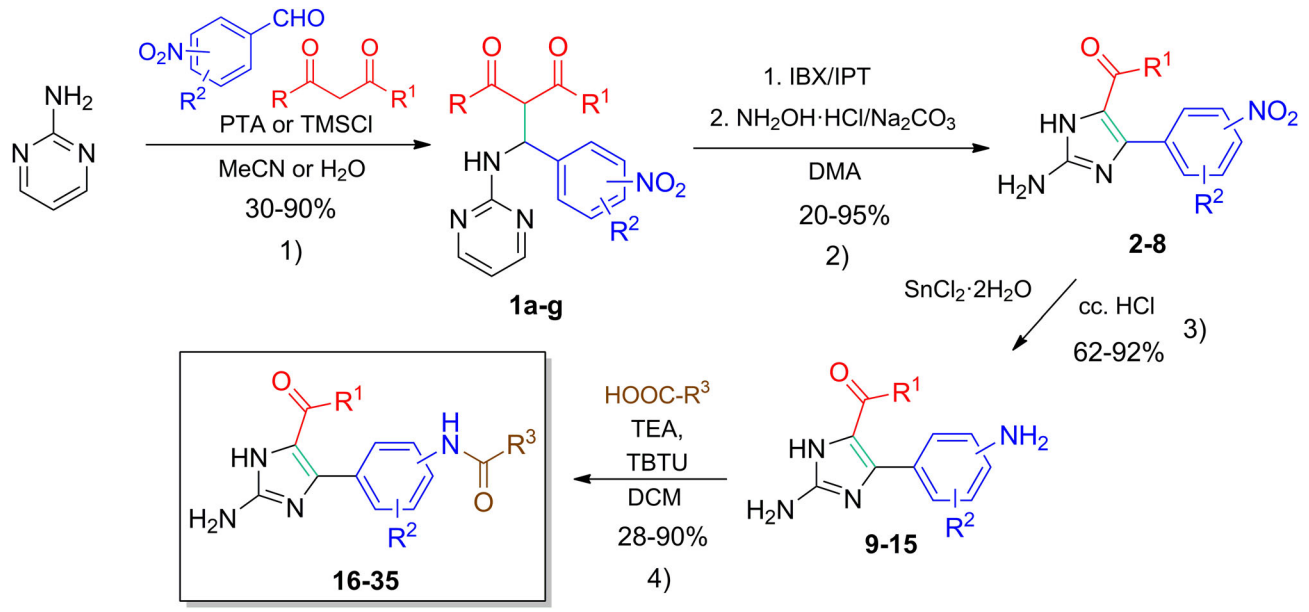

FIGURE 2 Four-step synthetic procedure towards the preparation of synthetic sponge alkaloid analogues **16–35** involving (1) Mannich 3-CR; Lewis acid -induced coupling reaction of 2-aminopyrimidine aldehydes and β-keto compounds; (2) Sequential one-pot, two-step annulation with formation of C4-, C5-disubstituted *2-amino-1H-imidazoles*; (3) Reduction of NO_2 group, preparation of 2-amino-4-aminophenyl-1*H*-imidazoles; (4) Coupling of the corresponding carboxylic acids furnishing the desired final products **16–35**

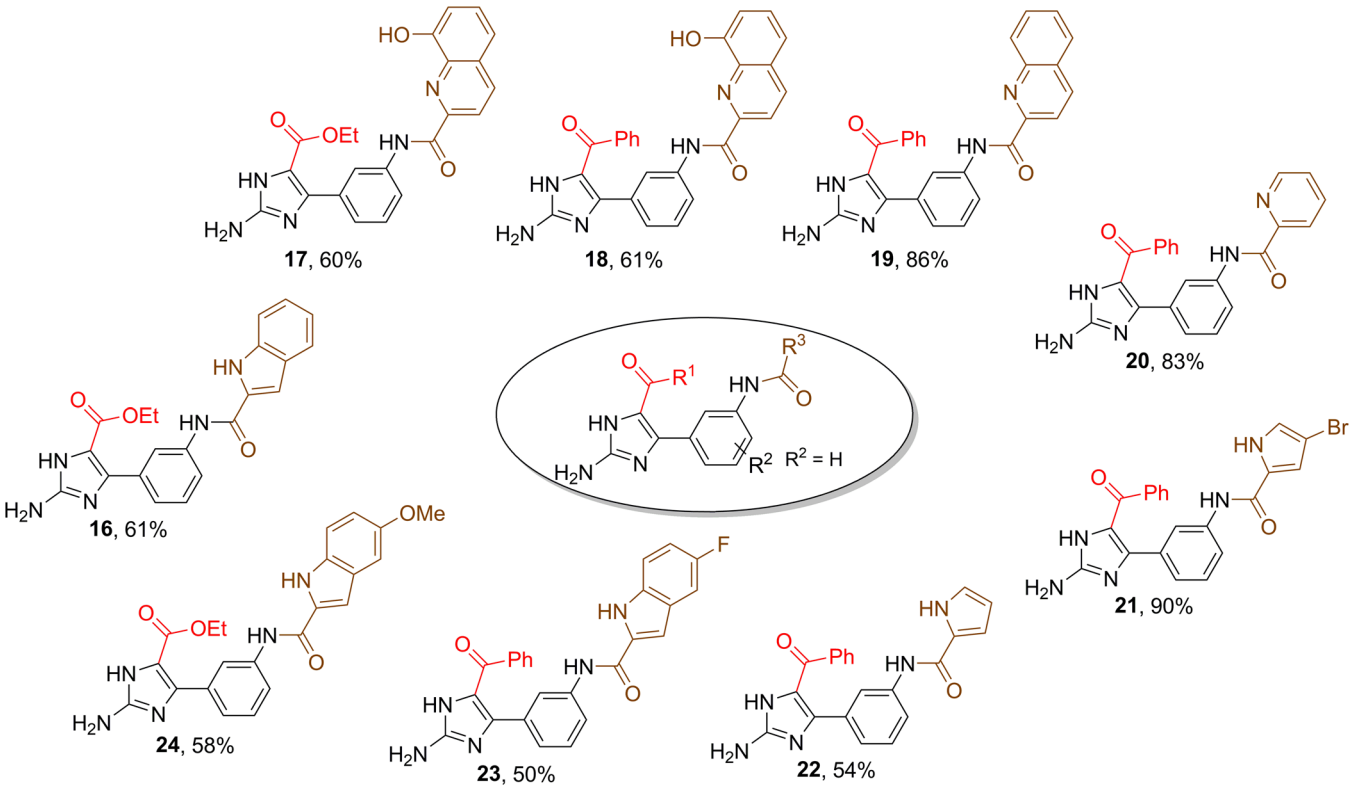

FIGURE 3 The structures of heterocycles **16–24** investigated in preliminary assessment. Compounds were synthesized by the above-mentioned protocol and were isolated in yields of 50%–90%

(for 23) or bromine (for **28**) resulted in significant increase of bioactivity in the same cells. Interestingly, the chlorine derivative (**29**) showed potent cytotoxicity in 4T1 cells (3.10 μM), but the fluorine (**23**) and brominated (**28**) derivatives exhibited lower cytotoxicity on 4T1 cells (9.05 or 12.99 μM), respectively. Similar HL-60 activity was observed for 23 (IC_{50} = 5.21 μM), 28 (IC_{50} = 2.91 μM), and 29 (IC_{50} = 4.03 μM). Surprisingly, 27 possessing a C-7-methoxy unit in the indole score (R^1 = Ph) presents comparable HL-60 result with a 3.12 μM IC_{50} value. On the other hand, diminished cytotoxicity was observed in those analogues, where R^1 = Me unit was introduced (**26** and **30**).

In consideration of the preparative and biological results, compound **28** has been selected for further structural modification from the three suitable analogues having acceptable cytotoxic effects in the range of 2.8–2.9 μM (target: HL-60 cell culture).

Diversification approaches included the addition of halogen and methyl substituents in different positions on the aromatic ring (with fixed R^1 position, compounds **32–34**); (Figure 5), or the precursor *meta* aminated form was changed into *para* (for **35**) leading to four analogues. As a result, only HL-60 inhibitory effect was observedfor **32** and **33**, exclusively (Figure 5). The observed 7.82 and 6.44 μM results revealed that any substitution of the aromatic ring reduced the cytotoxic potential even against the most sensitive HL-60 cell line.

3.2 | Compounds with 2-amino-1H-imidazol core impaired tumor cell viability

We defined the dose-response curves of our in-house synthetized 20-members compound library by the resazurin viability assay on 4T1 murine breast cancer, A549 human lung adenocarcinoma, and HL-60 human acute promyelocytic leukemia cells (Figure S2). The half maximal inhibitory concentration (IC_{50}) values are presented in Table 1. Several compounds not meeting criteria related to activity were omitted from further studies, these are as follows. The IC_{50} values of six compounds (**16, 20, 26, 30, 31, 34**) were above 10 μM (the pharmacologically favorable range) or the IC_{50} values of these compounds could not be determined (n.d.) for all three tested cell lines (Hughes et al., 2011). Two molecules were completely inactive in the applied concentration range (**19, 21**). Five compounds possessed low antiproliferative activity (**17, 18, 22, 24, 25**). Further investigations focused only on analogs with potent cytotoxic activity on three different cell lines: 4T1, A549, and HL-60. Seven compounds (**23, 27, 28, 29, 32, 33, 35**) that hampered the viability of all three tested cell lines were selected for subsequent experiments. The tumor cell specific cytotoxic selectivity of the compounds was tested on normal primary cells such as healthy human fibroblasts and PBMCs. While the 12.5 μM treatment with the selected seven compounds caused decline in the viability index to 0.7 of healthy human fibroblasts, the viability of PBMCs was not affected (Figure S3).

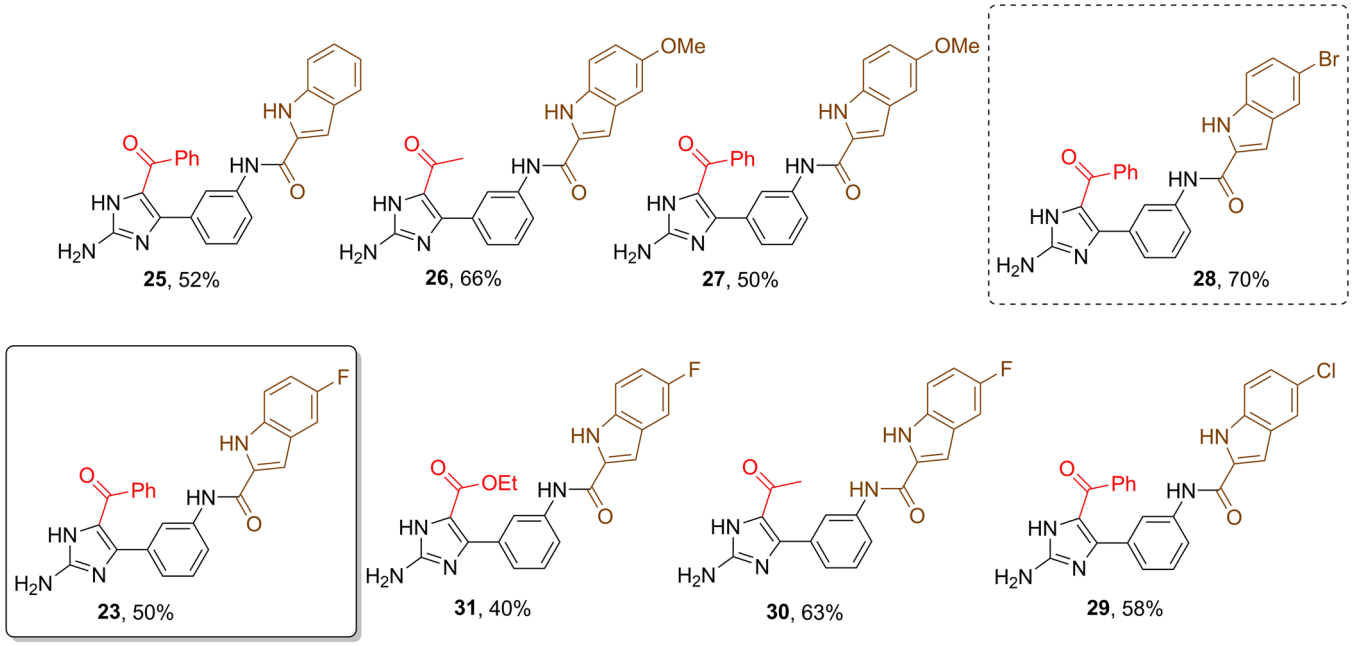

FIGURE 4 The chemical structures of the hit-like compound **23** and its descendant analogues **25–31**, isolating in yields of 40%–70%. Following the observed test results, the derivative **28** (dashed line box) was selected for further derivatization

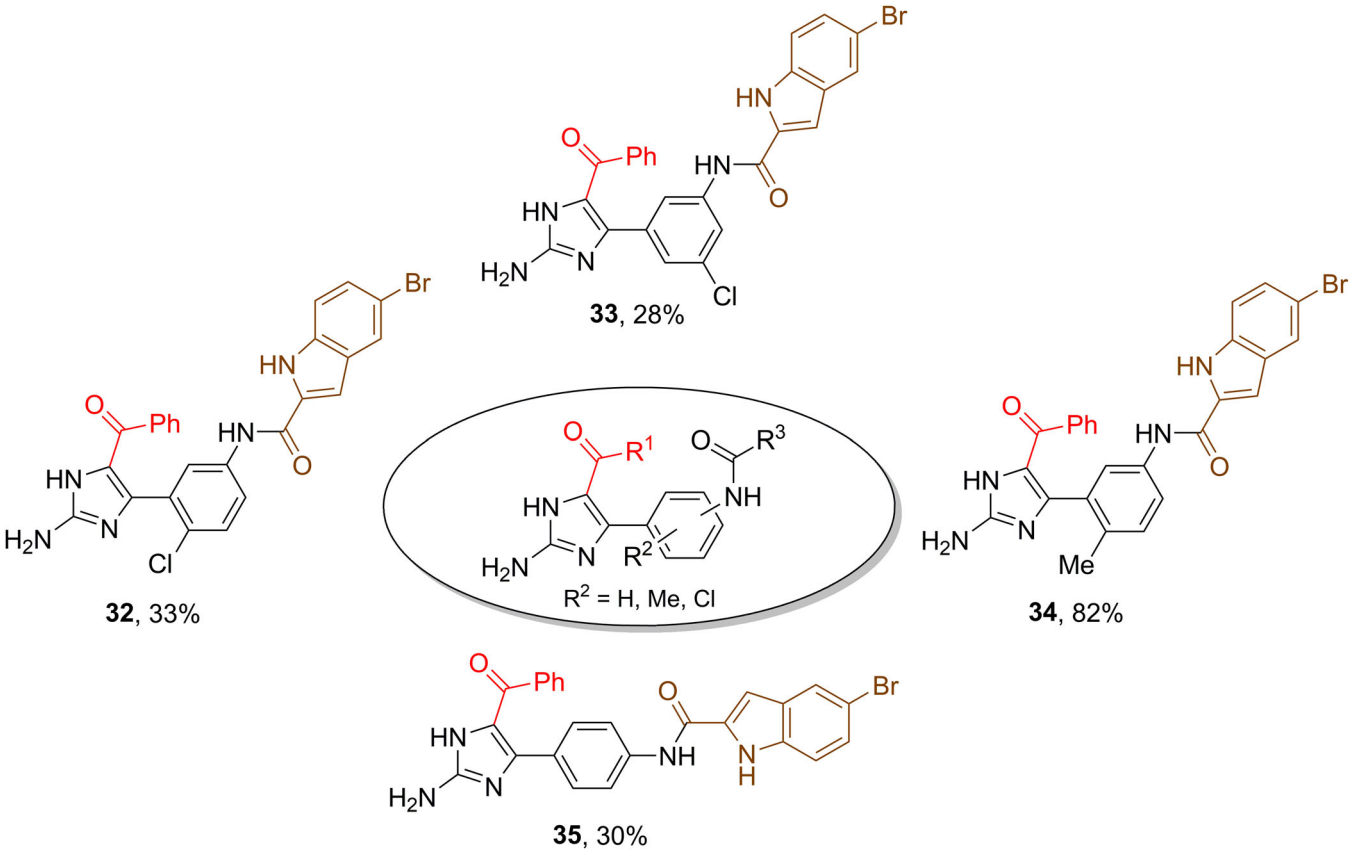

FIGURE 5 The results of late-stage structural modification of compound **28**. The synthesized four analogues **32–35** have isolated in yields of 28%–82%

TABLE 1 IC_{50} values (μM) of compounds 16–35 determined by resazurin assay

Compounds/ cells	4T1	A549	HL-60
16	19.32	34.63	14.42
17	17.11	n.d.	5.81
18	13.92	28.83	8.95
19	n.d.	n.d.	n.d.
20	30.69	n.d.	24.76
21	n.d.	n.d.	n.d.
22	n.d.	n.d.	6.90
23#	9.05	29.08	5.21
24	12.61	27.60	7.57
25	n.d.	n.d.	6.34
26	35.00	n.d.	24.80
27#	11.65	21.07	3.12
28#	12.99	15.62	2.91
29#	3.10	15.08	4.03
30	25.31	43.72	24.98
31	14.38	18.55	10.02
32#	12.44	20.27	7.82
33#	11.48	17.76	6.44
34	27.02	n.d.	24.30
35#	11.02	14.15	6.77

Note: Hashmark (#) labeled compounds were selected for further investigation. n.d. refers to "IC_{50} cannot be determined in the applied concentration range."

Cells were treated with compounds **16–35**, hashmark (#) labeled compounds were used in 39 nM, 78 nM, 1.56 μM, 3.125 μM, 6.25 μM, 12.5 μM concentrations and the following concentrations for the rest: 1.56, 3.125, 6.25, 12.5, 25, and 50 μM in three biological replicates for 72 h. Viability was examined by resazurin assay as described in Section 2.6. Materials and Methods. Hashmark (#) labeled compounds were selected for further investigation. n.d. refers to "IC_{50} cannot be determined in the applied concentration range."

3.3 | Compounds with 2-amino-1H-imidazol core induced apoptosis, phosphatydilserine exposure and sub-G1 increase in HL-60 cells

HL-60 human promyelocytic leukemia cells were the most sensitive for our marine sponge derivatives, therefore, HL-60 cells were selected for further study of the cytotoxic effect of the compounds. To clarify whether the viability of HL-60 cells was hampered by apoptosis or necrosis, we carried out annexin V-propidium iodide (PI) staining on the cells treated by the seven selected candidates (Figure 6a,b). 1, 3, and 6 μM treatments were used to apply a lower and higher concentration of the IC_{50} values of the compounds (**27**, **28**, and **29**) on HL-60 cells. Sponge alkaloid derivatives showed dose dependent phosphatidylserine exposure that suggests potent apoptotic activity (AnnV+/PI− early apoptosis and AnnV+/PI+ late apoptosis) in HL-60 cells (Figure 6c) without the appearance of a massive, only PI positive necrotic cell population (Figure 6c). 6 μM treatment of **23** caused a moderate apoptotic effect with 76.8 ± 3.5% living (*p < .05), 3.2 ± 0.7% early apoptotic (*p < .05), 15.5 ± 3.9% late apoptotic cells (*p < .05). The same 6 μM treatment with **27**, **28**, and **29** reduced the viability of HL-60 cells to 30.5 ± 0.7%, 31.1 ± 0.8%, and 37.8 ± 4.6%, respectively, compared to the viability of untreated samples (85 ± 3.9%, ***p<.001). After treatment with 6 μM **27**, **28,** and **29** early apoptotic cells were 16.1 ± 0.6%, 23.4 ± 1%, and 11.4 ± 1.1%, compared to the untreated samples (1.9 ± 0.5%, ***p < .001). After treatment with 6 μM **27**, **28,** and **29** late apoptotic cells were 50.7 ± 0.9%, 43.4 ± 1.2%, and 44.7 ± 4.8%, compared to the untreated samples (9.5 ± 2.7%, ***p < .001). The percentage of necrotic cell populations were unchanged after treatment with 6 μM **27**, **28,** and **29,** values were 2.5 ± 0.3%, 2.1 ± 0.4%, and 5.9 ± 1.1%, compared to untreated cells (3.6 ± 1.6%). 6 μM **32** or **33** reduced viability to 78.9 ± 1.6% or 79.1 ± 1.9% (*p < .05) and caused significant increase in late apoptotic cells with 11.7 ± 2.6% or 15.6 ± 1.8% (**p < .01) (Figure 6c). 6 μM **35** did not influenced AnnexinV translocation significantly after the 24 h incubation.

Apoptosis executed by the activation of caspases results in the internucleosomal degradation of genomic DNA which can be studied by flow cytometry as a hypodiploid sub-G1 fraction of the cell population. To confirm that apoptotic event we analyzed, the percentage of cells with degraded DNA, the sub-G1 fragment content of treated HL-60 cells was assayed after 72 h (Figure 7a,b). Our results showed that at a 6 μM treatment resulted in massive DNA degradation for **27**, **28**, and **29**. Cytotoxicity of the analogs resulted in DNA breakdown as the final step of apoptosis in a concentration dependent manner (Figure 7c). The 6 μM treatment with **23**, **27**, **28**, and **29** caused DNA fragmentation in 22.9 ± 1.2%, 53.8 ± 7.3%, 56.5 ± 2.8%, and 64.3 ± 2.1%, of HL-60 cells versus untreated control cells (11.7 ± 1.2%, ***p < .001) (Figure 7c).

3.4 | Apoptotic effect of compounds with 2-amino-1H-imidazol core does not exclusively rely on cytostatic effect rather the induction of mitochndrial membrane depolarization

In addition to cytotoxicity, we also investigated the cytostatic effect of our molecules on HL-60 cells. Compounds **23**, **28**, **32**, **33**, and **35** significantly disturbed cell cycle distribution of HL-60 cells. The cell cycle profile of HL-60 cells after 6 μM treatment with **27**, **28**, and **29** was not determinable because of the high degree of apoptosis after 72 h treatment. The arrest in G_2/M phase occurred upon incubation

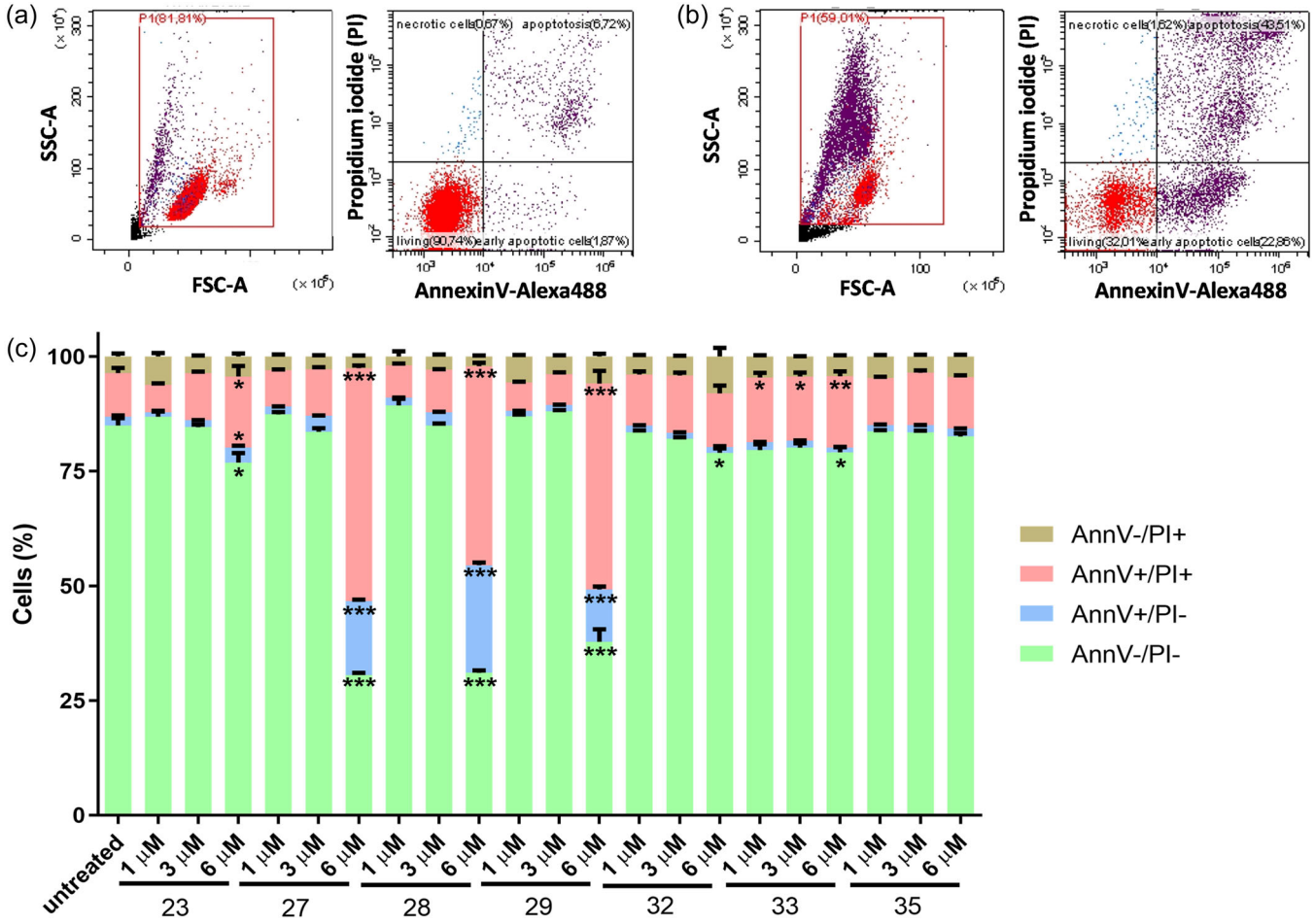

FIGURE 6 Sponge alkaloid analogs induced phosphatidylserine exposure. HL-60 leukemia cells were left untreated (a) or incubated with the compounds (b, example of 28 at 6 µM) as described in Section 2.7.1. Materials and Methods for 24 h. Representative dot plots are shown for gating and setting of quadrants (a, b). (c) The results are shown as arithmetic mean values of the early (AnnV+/PI−, blue column) and late apoptosis (AnnV+/PI+, pink column), living cells (AnnV−/PI−, green column), and necrotic cells (AnnV−/PI+, brown column) of three biological replicate samples ± *SD*, **p* < .05, ***p* < .01, ****p* < .001

with 3 µM **23** (22.4 ± 1.6%, ***p* < .01), 6 µM **23** (39.2 ± 3.1%, ****p* < .001), 3 µM **28** (21.0 ± 0.5%, ***p* < .01), 1 µM **35** (20.8 ± 0.4%, ***p* < .01) versus untreated control cells (17.3 ± 1.7%) (Figure 8b). The arrest in G_0/G_1 phase occurred upon incubation with **32** 1–6 µM and **33** 3–6 µM reaching a maximum (**33** at 6 µM) of 74.1 ± 1.4% versus 64.3 ± 1.9% of control cells.

However, there were statistical differences in the percentages of cells in different cell cycle phases, there were only moderate changes. On the other hand, the cell cycle arrest was only measurable after 72 h, subsequently of the previously demonstrated apoptotic PS exposure event, therefore authors speculate that induction of apoptosis is upstream of cell cycle disturbance. Therefore, another parameter confounding cellular viability, namely the mitochondrial homeostasis was assayed as early as 16 h following treatments. The perturbation of the cellular viability by the sponge alkaloid derivative compounds may confound the subcellular oxidative homeostasis affecting mitochondrial membrane potential (MMP). Mitochondrial membrane depolarization was examined by JC-1 (5,5′,6,6 tetrachloro-1,1′,3,3′-tetraethylbenzimidazolocarbocyanine iodide) staining following treatment of HL-60 cells. The JC-1 dye is in aggregated form with red color in cells with healthy mitochondria, but redox stress and mitochondrial membrane depolarization lead to the creation of JC-1 monomers with green color (Kanizsai et al., 2018). Our analogs depolarized mitochondria of HL-60 cells in a concentration dependent manner (Figure 9a,b). The four most cytotoxic compounds were selected for the MMP assay. The depolarizing effect of 3 µM **23**, **27**, **28**, and **29** compounds on MMP resulted 9.1 ± 0.2%, 13.3 ± 1.1% (***p* < .01), 10.4 ± 0.2% (***p* < .01), and 9.4 ± 1.1% cells with green JC-1 accumulation compared to the untreated 7.6 ± 0.6%, respectively. The depolarizing effect of 6 µM **23**, **27**, **28**, and **29** compounds on MMP resulted massive accumulation of 13.4 ± 0.8%, 42.4 ± 0.8%, 50.3 ± 0.7%, and 29.7 ± 2.1% cells with green JC-1 monomers compared to the untreated 7.6 ± 0.6%, respectively (****p* < .001).

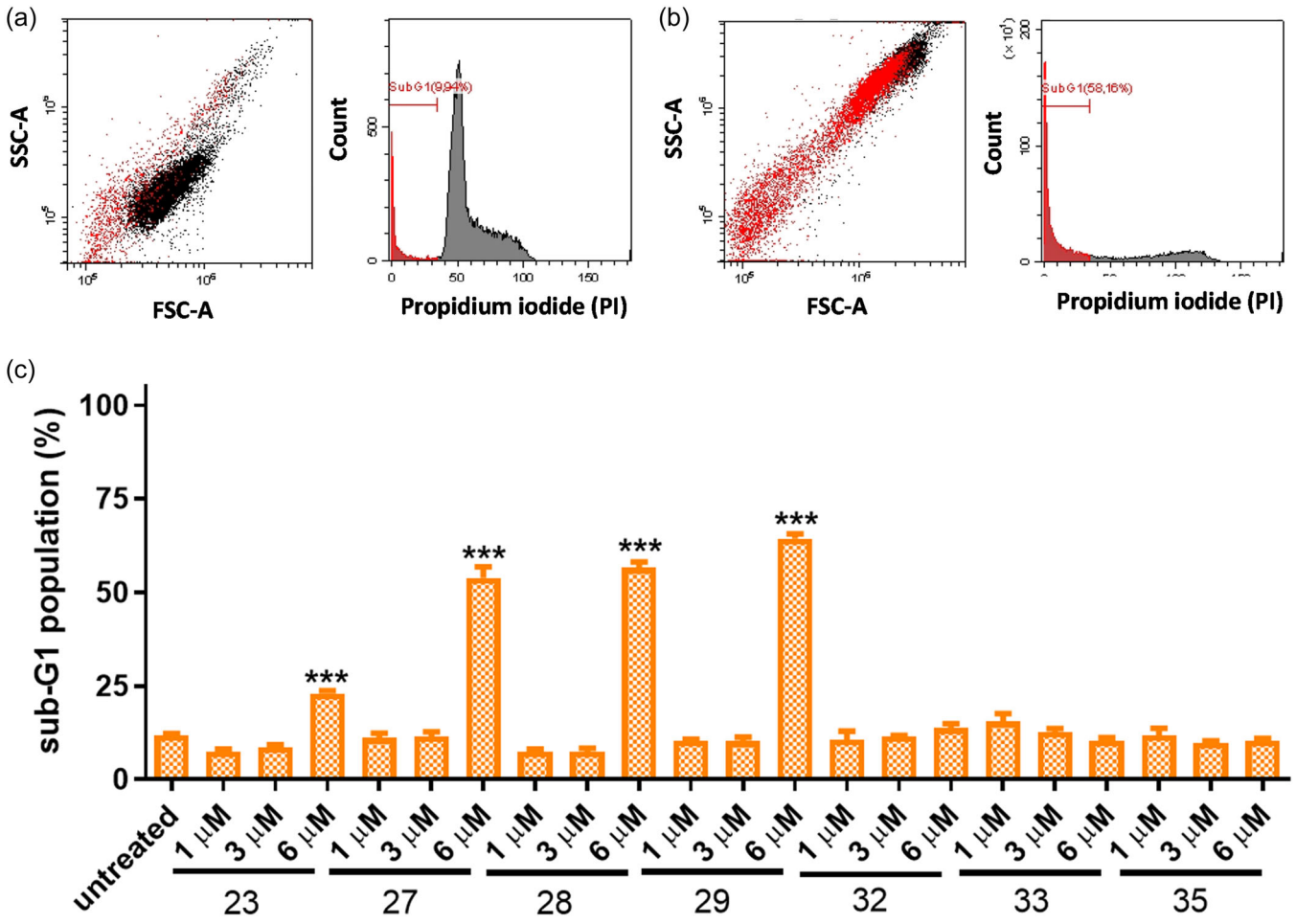

FIGURE 7 Analogs caused DNA breakdown and apoptosis of HL-60 cells. Representative SSC-FSC, and PI histograms are presented where cells were left untreated (a) or treated for 72 h (b, example of **28** at 6 μM). (c) The arithmetic mean values of three biological replicates ± *SD* are presented. Cells were treated with the alkaloid derivatives with the indicated concentrations (μM) in the figure in duplicates for 72 h. Sub-G1 population was analyzed by flow cytometry as described in Section 2.7.2 (Materials and methods). $^{*}p < .05$, $^{**}p < .01$, $^{***}p < .001$.

3.5 | Lead compound inhibited the A549 human lung carcinoma and 4T1 murine breast tumor growth

Taken together the data about the synthesis, solubility, and apoptotic effects of our compounds, **28** and **29** were selected for in vivo studies with the potential of tumor growth inhibition. First, the orthotopic and syngeneic 4T1 triple negative breast cancer model was assayed. Compound **28** reduced 4T1 tumor volume to 675 ± 139 mm^3 by the 28th day, but without statistical significance (Figure 10a). On the 27th day of tumor growth, **29** had significant 4T1 tumor growth inhibition reducing tumor volume to 443 ± 54 mm^3 ($^{*}p < .05$) compared to untreated mice with 768 ± 134 mm^3 tumor volume (Figure 10b). Cisplatin was more effective than our compounds in the 4T1 model reducing tumor growth to 245 ± 45 mm^3 ($^{**}p < .01$) by the 28th day compared to the average tumor volume of the untreated group with 939 ± 162 mm^3 (Figure 10a,b). The **28** was tested on the A549 xenograft model reducing tumor growth to 354 ± 15 mm^3 compared to untreated mice with 553 ± 66 mm^3 ($^{*}p < .05$). Cisplatin showed the same effectivity inhibiting A549 tumor growth as **28** with the average tumor volume of 368 ± 23 mm^3 by the day of 46th ($^{*}p < .05$) (Figure 10c).

4 | DISCUSSION

Despite the advent of the integration of immunotherapy and targeted therapy into the arsenal of traditional anticancer interventions (such as surgery, radiotherapy, chemotherapy), cancer remained one of the deadliest disease groups with high need for novel therapies (Advancing Cancer Therapy, 2021; Akkin et al., 2021; Zhong et al., 2021). Since 70% of the planet is covered by oceans, marine organism may serve a wide inventory of bioactive compounds. Almost 78% of the chemotherapeutic agents are isolated form natural source or synthetized from naturally occurring scaffolds (LaBarbera et al., 2009). Sponges (phylum *Porifera*) as sessile organisms without adaptive immune cells, protect against pathogens and invaders by the synthesis of seconder metabolites, alkaloids.

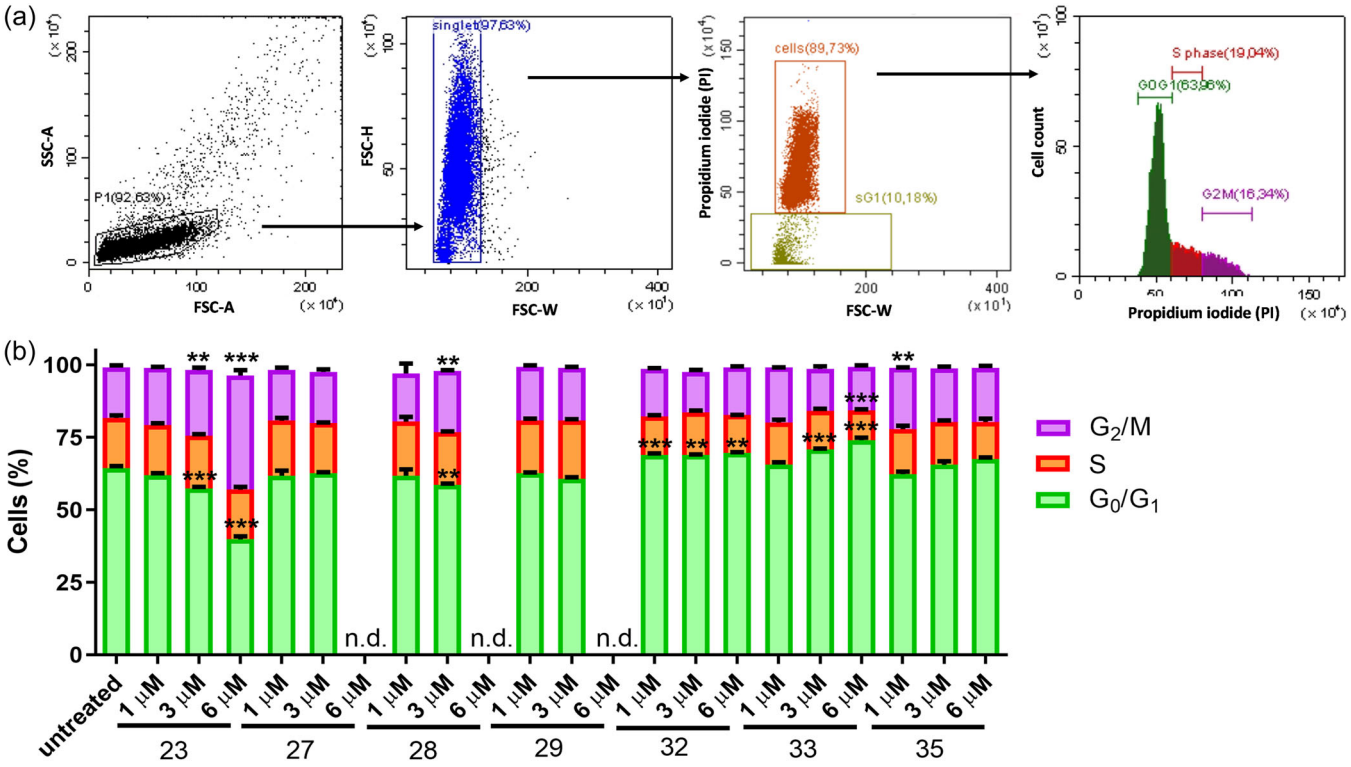

FIGURE 8 Compounds With *2-Amino-1H-Imidazol* Core caused G_2/M arrest of HL-60 cells. (a) Representative dot plots are presented for gating out debris and aggregates by SSC-FSC plots, gating singlets by FSC-H/FSC-W plots, and gating cells by PI/FSC-W plots. Cells were treated with compounds with the indicated concentrations (μM) in the figure and G_0/G_1, S, G_2/M cell cycle phase distributions were analyzed by flow cytometry as described in Section 2.7.2 (Materials and Methods). (b) The results are shown as arithmetic mean values of three biological replicate samples ± *SD*, * $p < .05$; ** $p < .01$; *** $p < .001$. n.d. refers to samples with not determinable cell cycle distribution due to high degree of apoptosis

We have demonstrated a multistep synthetic pathway preparing synthetic sponge alkaloids decorating at C-4 and C-5 position with (hetero)aromatic units for 2-AI score. The newly synthesized species were observed in acceptable yields, in addition, the developed method is available for a construction of higher membered chemical library diversifying in arbitrary combinations. From our established 20-membered library, eighteen of 20 compounds showed cytotoxic effect on the cancer cell lines with different potential. As structure-activity relationship revealed that introducing of quinoline and pyrrole moieties at R3 position diminished or decreased the cytotoxic behavior, similarly to the pyridine unit. Although the unsubstituted indole ring showed a poor activity, any modification on the adjacent phenyl group at C-7 with either EWG (halogenides) or ED (OMe) group led to significant improvement of cytotoxic efficiency. In addition, changes of R1 position such as OEt→ phenyl or Me have increased the antitumor potential as demonstrating C-7 fluorine as well as methoxy substituted variants. As a conclusion, the presence of C-7-halogene such as fluorine (**23**), bromine (**28**), or chlorine (**29**) as well as EWG moiety including methoxy (**27**) substituted indole and R1= Ph contributed for the highest cytotoxic potential.

Healthy controls cells, such as healthy human fibroblasts and PBMCs were treated with our compounds to exclude general cytotoxicity. Viability of healthy fibroblasts and PBMCs upon treatment was less hampered compared to cancer cell lines supporting tumor cell specific cytotoxicity of our compounds. However, the most cytotoxic compounds resulted the following IC_{50} values 28: 2.91 μM on HL-60 cells, and 29: 3.1 μM on 4T1 cells. The A549 cells were less sensitive to the treatments with IC_{50} 15 μM for both 28 and 29. Single cell flow cytometry was used to further investigate the effects of our compounds on the tested cell lines. Flow cytometry demonstrated the apoptotic effect of the most active seven compounds inducing phosphatidylserine exposure and sub-G1 fragmentation of nuclear DNA. FDA approved DNA base analogues (Fludarabine, Nelarabine, Cyterabine) blocks S-phase, therefore, cell cycle arrest was observed, but our compounds had moderate effect on this. Although, microtubule destabilizer effect of our compounds was not assayed, it is quite unlikely since only moderate changes were detected in cell cycle distributions upon treatment. Conversely, the mitochondrial red/ox homeostasis was hampered quite early in our experiments since four compounds caused depolarization of the MMP as an early event of apoptosis after 16 h treatment. The observed proapoptotic effects of our compounds are in great agreement with previous studies of marine sponge alkaloids. The anticancer effect, induction of the intrinsic apoptotic pathway via mitochondrial membrane depolarization upon treatment with different marine sponge alkaloids was previously reviewed by others

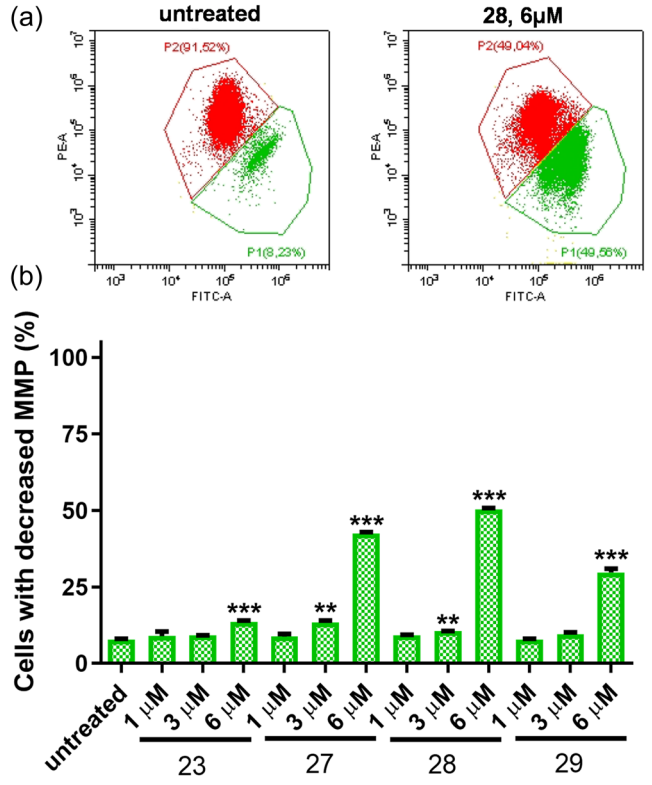

FIGURE 9 Compounds depolarized mitochondria of HL-60 cells examined by JC-1 staining. (a) Representative PE (red)/FITC (green) dot plots and (b) arithmetic means of percentages of three biological replicates (±*SD*) of cells with decreased MMP at 16 h following treatment. JC-1 was analyzed by flow cytometry as described in Section 2.7.2, $^{*}p < .05$, $^{**}p < .01$, $^{***}p < .001$

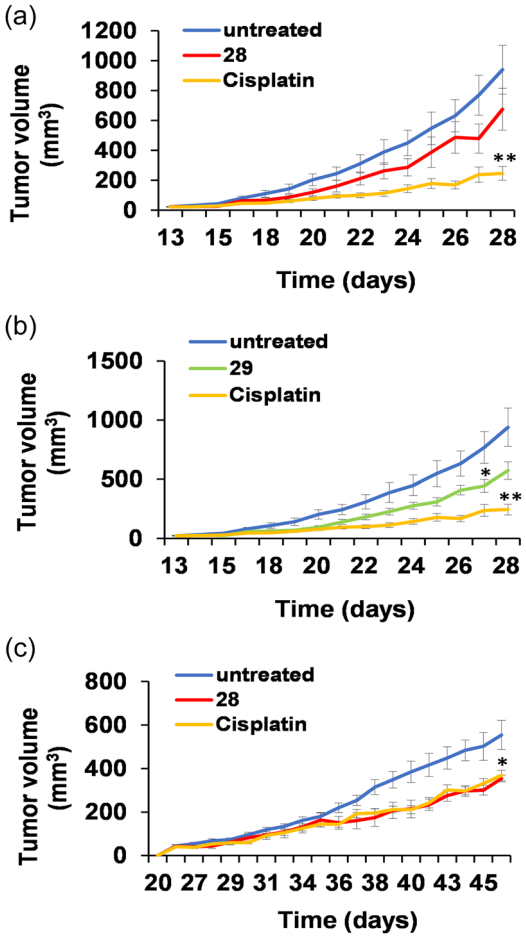

FIGURE 10 Tumor growth rate of 4T1 murine triple negative breast cancer (a, b) and A549 human lung adenocarcinoma (c) was inhibited by our compounds. Animals were injected with the tumor cells, treated with the compounds (**28** or **29**) and daily monitored as described in the Section 2.8 (Materials and Methods). Cisplatin was used as a standard of care, $n = 10$/group. The arithmetic means and SEM values are represented of the tumor volume (mm^3). SEM, standard error of the mean

(Barreca et al., 2020; Calcabrini et al., 2017; Munekata et al., 2021). Naamidine A, a sponge alkaloid was early reported to exert apoptotic effects in the A431 epidermoid carcinoma cancer cell line following a 15 μM treatment (LaBarbera et al., 2009). Another sponge compound, (−)-Agelasidine A also demonstrated Annexin V+ apoptosis and mitochondrial membrane depolarization in Hep3B hepatocellular carcinoma cells treated with 35 μM for 24 h (Lu et al., 2022). Other sponge alkaloids such as, Hemimycalin C, Hemimycalin D, and Hemimycalin E were recently reviewed as antiproliferative agents in the colorectal cancer cell line HCT-116 with 18.6, 17.1, and 8.6 μM IC_{50} values, respectively (Han et al., 2022).

Importantly, marine sponge alkaloid derivatives, synthetized in our laboratory showed superior antiproliferative, apoptotic effects on the tested cancer cell lines compared to previously described molecules and their effects were comparable in efficiency to cisplatin in reducing tumor growth in two rodent tumor models. The two tumor models were significantly different in that, the first utilized human lung adenocarcinoma, A549 cells injected subcutaneously into immunodeficient mice. While the other was a syngeneic model with 4T1 mouse breast cancer, cells injected orthotopically into the mammary fat pad in immunocompetent mice. These murine tumor models, considering their advantages and limitations, showed not only general applicability but also shed light on the comparable tumor growth inhibitory effects of our derivatives (**28**, **29**) with the golden standard cisplatin. Further chemical modifications of our derivatives along the obtained SAR data may provide potential anticancer agents containing natural sponge alkaloid scaffolds.

AUTHOR CONTRIBUTIONS

Conceptualization: Iván Kanizsai, Gábor J. Szebeni, and László. G. Puskás; *Methodology*: Nikolett Gémes, Zsófia Makra, Patrícia Neuperger, Enikő Szabó, and József Á. Balog; *Software*: Nikolett Gémes, Iván Kanizsai, and Gábor J. Szebeni; *Validation*: Nikolett Gémes, Zsófia Makra, and László Hackler; *Formal analysis*: Nikolett Gémes; *Investigation*: Nikolett Gémes, Zsófia Makra, Patrícia Neuperger, Enikő Szabó, József Á. Balog, Lili Borbála Flink, and Beáta Kari; *Resources*: László. G. Puskás; *Data curation*: Iván Kanizsai, Gábor J. Szebeni; *Writing—original draft preparation*: Iván Kanizsai, and Gábor J. Szebeni; *Writing—review and editing*: Iván Kanizsai, László Hackler, Gábor J. Szebeni, and László.

G. Puskás; *Visualization*: Nikolett Gémes, Zsófia Makra, Iván Kanizsai, and Gábor J. Szebeni; *Supervision*: Iván Kanizsai, Gábor J. Szebeni, and László. G. Puskás; *Project administration*: László. G. Puskás; *Funding acquisition*: Gábor J. Szebeni, and László. G. Puskás. All authors have read and agreed to the published version of the manuscript.

ACKNOWLEDGMENTS

This research was funded by the 2020-1.1.6-JÖVŐ–2021-00003 and 142877 FK22 (GJS) grant from the National Research, Development, and Innovation Office (NKFI), Hungary. This work was supported by the ÚNKP-22-5 -SZTE-535 (GJS) New National Excellence Program of the Ministry for Innovation and Technology from the source of the National Research, Development and Innovation Fund. This work was supported by the János Bolyai Research Scholarship of the Hungarian Academy of Sciences BO/00582/22/8 (GJS).

CONFLICTS OF INTEREST

ZM, BK, LH, and IK are employees of Avidin Ltd. LGP is the CEO of Avidin Ltd. The other authors declare no conflicts of interest.

DATA AVAILABILITY STATEMENT

Raw data or additional data are available from the corresponding authors upon request.

ORCID

Iván Kanizsai https://orcid.org/0000-0003-0109-7097
Gábor J. Szebeni https://orcid.org/0000-0002-6998-5632

REFERENCES

Advancing Cancer Therapy. (2021). *Nature Cancer*, *2*, 245–246.

Akkin, S., Varan, G., & Bilensoy, E. (2021). A review on cancer immunotherapy and applications of nanotechnology to chemoimmunotherapy of different cancers. *Molecules*, *26*(11), 3382.

Alfoldi, R., Balog, J. A., Farago, N., Halmai, M., Kotogany, E., Neuperger, P., Nagy, L. I., Fehér, L. Z., Szebeni, G. J., & Puskás, L. G. (2019). Single cell mass cytometry of non-small cell lung cancer cells reveals complexity of in vivo and three-dimensional models over the petri-dish. *Cells*, *8*(9), 1093.

Anjum, K., Abbas, S. Q., Shah, S. A., Akhter, N., Batool, S., & Hassan, S. S. (2016). Marine sponges as a drug treasure. *Biomolecules & Therapeutics*, *24*, 347–362.

Balog, J. A., Hackler Jr, L., Kovacs, A. K., Neuperger, P., Alfoldi, R., Nagy, L. I., Puskás, L. G., & Szebeni, G. J. (2019). Single cell mass cytometry revealed the immunomodulatory effect of cisplatin via downregulation of splenic CD44+, IL-17A+ MDSCs and promotion of circulating IFN-gamma+ myeloid cells in the 4T1 metastatic breast cancer model. *International Journal of Molecular Sciences*, *21*(1), 170.

Barreca, M., Spano, V., Montalbano, A., Cueto, M., Diaz Marrero, A. R., Deniz, I., Erdoğan, A., Bilela, L. L., Moulin, C., Taffin-de-Givenchy, E., Spriano, F., Perale, G., Mehiri, M., Rotter, A., Thomas, O. P., Barraja, P., Gaudêncio, S. P., & Bertoni, F. (2020). Marine anticancer agents: An overview with a particular focus on their chemical classes. *Marine Drugs*, *18*(12), 619.

Berdis, A. J. (2017). Inhibiting DNA polymerases as a therapeutic intervention against cancer. *Frontiers in Molecular Biosciences*, *4*, 4.

Berlinck, R. G. S., & Kossuga, M. H. (2005). Natural guanidine derivatives. *Natural Product Reports*, *22*, 516–550.

Boucle, S., Melin, C., Clastre, M., & Guillard, J. (2015). Design, synthesis and evaluation of new marine alkaloid-derived pentacyclic structures with anti-tumoral potency. *Marine Drugs*, *13*, 655–665.

Calcabrini, C., Catanzaro, E., Bishayee, A., Turrini, E., & Fimognari, C. (2017). Marine sponge natural products with anticancer potential: An updated review. *Marine Drugs*, *15*(10), 310.

Chaudhary, V., Venghateri, J. B., Dhaked, H. P. S., Bhoyar, A. S., Guchhait, S. K., & Panda, D. (2016). Novel Combretastatin-2-aminoimidazole analogues as potent tubulin assembly inhibitors: exploration of unique pharmacophoric impact of bridging skeleton and aryl moiety. *Journal of Medicinal Chemistry*, *59*, 3439–3451.

Chong, P., Sebahar, P., Youngman, M., Garrido, D., Zhang, H., Stewart, E. L., Nolte, R. T., Wang, L., Ferris, R. G., Edelstein, M., Weaver, K., Mathis, A., & Peat, A. (2012). Rational design of potent non-nucleoside inhibitors of HIV-1 reverse transcriptase. *Journal of Medicinal Chemistry*, *55*, 10601–10609.

Curbo, S., & Karlsson, A. (2006). Nelarabine: A new purine analog in the treatment of hematologic malignancies. *Reviews on Recent Clinical Trials*, *1*, 185–192.

Dalmartello, M., La Vecchia, C., Bertuccio, P., Boffetta, P., Levi, F., Negri, E., & Malvezzi, M. (2022). European cancer mortality predictions for the year 2022 with focus on ovarian cancer. *Annals of Oncology*, *33*, 330–339.

Demjen, A., Alfoldi, R., Angyal, A., Gyuris, M., Hackler Jr, L., Szebeni, G. J., Wölfling, J, Puskás, L. G., & Kanizsai, I. (2018). Synthesis, cytotoxic characterization, and SAR study of imidazo[1,2-b]pyrazole-7-carboxamides. *Archiv der Pharmazie (Weinheim)*, *351*, e1800062.

Dybdal-Hargreaves, N. F., Risinger, A. L., & Mooberry, S. L. (2015). Eribulin mesylate: Mechanism of action of a unique microtubule-targeting agent. *Clinical Cancer Research*, *21*, 2445–2452.

Dyson, L., Wright, A. D., Young, K. A., Sakoff, J. A., & McCluskey, A. (2014). Synthesis and anticancer activity of focused compound libraries from the natural product lead, oroidin. *Bioorganic & Medicinal Chemistry*, *22*, 1690–1699.

Elgoud Said, A. A., Mahmoud, B. K., Attia, E. Z., Abdelmohsen, U. R., & Fouad, M. A. (2021). Bioactive natural products from marine sponges belonging to family Hymedesmiidae. *RSC Advances*, *11*, 16179–16191.

Elissawy, A. M., Soleiman Dehkordi, E., Mehdinezhad, N., Ashour, M. L., & Mohammadi Pour, P. (2021). Cytotoxic alkaloids derived from marine sponges: A comprehensive review. *Biomolecules*, *11*, 258.

Ercolano, G., De Cicco, P., & Ianaro, A. (2019). New drugs from the sea: Pro-apoptotic activity of sponges and algae derived compounds. *Marine Drugs*, *17*, 31.

Han, N., Li, J., & Li, X. (2022). Natural marine products: Anti-colorectal cancer in vitro and in vivo. *Marine Drugs*, *20*(6), 349.

Hoffmann, H., & Lindel, T. (2003). Synthesis of the pyrrole-imidazole alkaloids. *Synthesis-Stuttgart*, *2003*, 1753–1783.

Hughes, J., Rees, S., Kalindjian, S., & Philpott, K. (2011). Principles of early drug discovery. *British Journal of Pharmacology*, *162*, 1239–1249.

Hura, N., Sawant, A. V., Kumari, A., Guchhait, S. K., & Panda, D. (2018). Combretastatin-Inspired heterocycles as antitubulin anticancer agents. *ACS Omega*, *3*, 9754–9769.

Kanizsai, I., Madácsi, R., Hackler Jr, L., Gyuris, M., Szebeni, G. J., Huzián, O., & Puskás, L. G. (2018). Synthesis and cytoprotective characterization of 8-hydroxyquinoline betti products. *Molecules*, *23*, 1934.

Kotogany, E., Balog, J. A., Nagy, L. I., Alfoldi, R., Bertagnolo, V., Brugnoli, F., Demjén, A., Kovács, A. K., Batár, P., Mezei, G., Szabó, R., Kanizsai, I., Varga, C., Puskás, L. G., & Szebeni, G. J. (2020). Imidazo[1,2-b]pyrazole-7-carboxamide derivative induces differentiation-coupled apoptosis of immature myeloid cells such as acute myeloid leukemia and myeloid-derived suppressor cells. *International Journal of Molecular Sciences*, *21*(14), 5135.

LaBarbera, D. V., Modzelewska, K., Glazar, A. I., Gray, P. D., Kaur, M., Liu, T., Grossman, D., Harper, M. K., Kuwada, S. K., Moghal, N., & Ireland, C. M. (2009). The marine alkaloid naamidine A promotes caspase-dependent apoptosis in tumor cells. *Anti-Cancer Drugs*, *20*, 425–436.

Lu, I. T., Lin, S. C., Chu, Y. C., Wen, Y., Lin, Y. C., Cheng, W. C., Sheu, J.-H., & Lin, C.-C. (2022). (-)-Agelasidine A induces endoplasmic reticulum stress-dependent apoptosis in human hepatocellular carcinoma. *Marine Drugs*, *20*(2), 109.

Makra, Z., Bényei, A., Puskás, L. G., & Kanizsai, I. (2020). One-pot access towards 4,5-Disubstituted 2-amino-1H-imidazoles starting from mannich substrates and their transformation utilities. *European Journal of Organic Chemistry*, *2020*, 7184–7196.

Munekata, P. E. S., Pateiro, M., Conte-Junior, C. A., Dominguez, R., Nawaz, A., Walayat, N., Fierro, E. M., & Lorenzo, J. M. (2021). Marine alkaloids: Compounds with in vivo activity and chemical synthesis. *Marine Drugs*, *19*, 374.

Nagasawa, K., & Hashimoto, Y. (2003). Synthesis of marine guanidine alkaloids and their application as chemical/biological tools. *The Chemical Record*, *3*, 201–211.

Puskás, L. G., Mán, I., Szebeni, G., Tiszlavicz, L., Tsai, S., & James, M. A. (2016). Novel Anti-CRR9/CLPTM1L antibodies with antitumorigenic activity inhibit cell surface accumulation, PI3K interaction, and survival signaling. *Molecular Cancer Therapeutics*, *15*, 985–997.

Sarfati, D., & Gurney, J. (2022). Preventing cancer: The only way forward. *The Lancet*, *400*, 540–541.

Su, Z., Yeagley, A. A., Su, R., Peng, L., & Melander, C. (2012). Structural studies on 4,5-Disubstituted 2-aminoimidazole-based biofilm modulators that suppress bacterial resistance to β-Lactams. *ChemMedChem*, *7*, 2030–2039.

Sung, H., Ferlay, J., Siegel, R. L., Laversanne, M., Soerjomataram, I., Jemal, A., & Bray, F. (2021). Global cancer statistics 2020: GLOBOCAN estimates of incidence and mortality worldwide for 36 cancers in 185 countries. *CA: A Cancer Journal for Clinicians*, *71*, 209–249.

Szebeni, G. J., Balog, J. A., Demjén, A., Alföldi, R., Végi, V. L., Fehér, L. Z., Mán, I., Kotogány, E., Gubán, B., Batár, P., Hackler Jr, L., Kanizsai, I., & Puskás, L. G. (2018). Imidazo[1,2-b]pyrazole-7-carboxamides induce apoptosis in human leukemia cells at nanomolar concentrations. *Molecules*, *23*, 2845.

Szebeni, G. J., Balazs, A., Madarasz, I., Pocz, G., Ayaydin, F., Kanizsai, I., Fajka-Boja, R., Alföldi, R., Hackler Jr, L., & Puskás, L. G. (2017). Achiral Mannich-base curcumin analogs induce unfolded protein response and mitochondrial membrane depolarization in PANC-1 cells. *International Journal of Molecular Sciences*, *18*(10), 2105.

Szebeni, G. J., Gémes, N., Honfi, D., Szabó, E., Neuperger, P., Balog, J. Á., Nagy, L. I., Szekanecz, Z., Puskás, L. G., Toldi, G., & Balog, A. (2022). Humoral and cellular immunogenicity and safety of five different SARS-CoV-2 vaccines in patients with autoimmune rheumatic and musculoskeletal diseases in remission or with low disease activity and in healthy controls: A single center study. *Frontiers in Immunology*, *13*, 846248.

Tomašič, T., Nabergoj, D., Vrbek, S., Zidar, N., Jakopin, Ž., Žula, A., Hodnik, Ž., Jukič, M., Anderluh, M., Ilaš, J., Dolenc, M. S., Peluso, J., Ubeaud-Séquier, G., Muller, C. D., Mašič, L. P., & Kikelj, D. (2015). Analogues of the marine alkaloids oroidin, clathrodin, and hymenidin induce apoptosis in human HepG2 and THP-1 cancer cells. *MedChemComm*, *6*, 105–110.

Wang, E., Sorolla, M. A., Gopal Krishnan, P. D., & Sorolla, A. (2020). From seabed to bedside: A review on promising marine anticancer compounds. *Biomolecules*, *10*, 248.

Weinreb, S. M. (2007). Some recent advances in the synthesis of polycyclic imidazole-containing marine natural products. *Natural Product Reports*, *24*, 931–948.

Wiese, M., & Daver, N. (2018). Unmet clinical needs and economic burden of disease in the treatment landscape of acute myeloid leukemia. *The American Journal of Managed Care*, *24*, 347.

Ye, J., Zhou, F., Al-Kareef, A. M. Q., & Wang, H. (2015). Anticancer agents from marine sponges. *Journal of Asian Natural Products Research*, *17*, 64–88.

Zhong, L., Li, Y., Xiong, L., Wang, W., Wu, M., Yuan, T., Yang, W., Tian, C., Miao, Z., Wang, T., & Yang, S. (2021). Small molecules in targeted cancer therapy: Advances, challenges, and future perspectives. *Signal Transduction and Targeted Therapy*, *6*, 201.

Zidar, N., Montalvão, S., Hodnik, Ž., Nawrot, D., Žula, A., Ilaš, J., Kikelj, D., Tammela, P., & Mašič, L. (2014). Antimicrobial activity of the marine alkaloids, clathrodin and oroidin, and their synthetic analogues. *Marine Drugs*, *12*, 940–963.

SUPPORTING INFORMATION

Additional supporting information can be found online in the Supporting Information section at the end of this article.

How to cite this article: Gémes, N., Makra, Z., Neuperger, P., Szabó, E., Balog, J. Á., Flink, L. B., Kari, B., Hackler Jr, L., Puskás, L. G., Kanizsai, I., & Szebeni, G. J. (2022). A cytotoxic survey on *2-amino-1H-imidazol* based synthetic marine sponge alkaloid analogues. *Drug Development Research*, 83, 1906–1922. https://doi.org/10.1002/ddr.22006